METHYLATION OF PHENOL OVER HIGH-SILICA BETA ZEOLITE
Effect of zeolite acidity and crystal size on catalyst behaviour

M.Bregolato[a], V.Bolis[b], C.Busco[b], P. Ugliengo[c], S.Bordiga[c], F.Cavani[d], N.Ballarini[d], L.Maselli[d], S.Passeri[d], I.Rossetti[a] and L.Forni[a] *

[a] Dip. Chimica Fisica ed Elettrochimica, Università di Milano, via C. Golgi 19, I-20133 Milano and INSTM, Research Unit of Milano, Italy
[b] Dip. DiSCAFF, Università del Piemonte Orientale "A. Avogadro", Via G. Bovio 6, I-28100 Novara, INSTM, Research Unit of Piemonte Orientale and NIS Centre of Excellence, Italy
[c] Dip. Chimica IFM, Università di Torino, via P. Giuria 7, I-10125 Torino, INSTM, Research Unit of Torino and NIS Centre of Excellence, Italy
[d] Dip. Chimica Industriale e dei Materiali, Università di Bologna, v.le Risorgimento 4, I-40136 Bologna and INSTM, Research Unit of Bologna, Italy. A Partner of Idecat NoE, 6FP of the EU.

ABSTRACT

A systematic investigation has been carried out, aiming at elucidating several aspects of the gas/solid methylation of phenol over high Si/Al ratio BEA-structured zeolite in protonated form. The catalysts have been characterized by several techniques, such as XRD, SEM, BET, ICP, FT-IR, TGA, micro-calorimetry and modelling by *ab initio* calculations. The correlation between these characteristics and kinetics and mechanistic features of the catalytic reaction, as well as of catalyst deactivation, showed that these zeolites are very active for the present reaction, leading to cresols and anisole as primary products. As catalyst deactivation proceeds, the selectivity to cresols and anisole increases substantially, together with a rapid decrease of selectivity to poly-alkylated species. Catalyst surface acidity is prevalently made of medium-to-low-strength silanols-based acid sites of Brønsted type. High-strength Lewis acid sites are either almost absent, especially when metal cations partially substitute for protons, or play a role essentially in catalyst deactivation. Stacking faults in the zeolite framework, generated by the

intergrowth of at least two BEA polymorphs, lead to an increase of the concentration of silanols-based acid sites. Deactivation is essentially due to the interaction of phenol and oxygenated products with the strong Lewis acid sites. For time-on stream values longer than a few hours, self oligomerisation-cyclisation of methanol to olefins and aromatics, followed by further alkylation to aromatic C atoms, contributes more significantly to catalyst deactivation. At higher temperature all the zeolites deactivate at a comparable rate, whereas at lower temperature initial catalytic activity is higher for larger crystal size zeolite, due to the longer diffusion time of bulkier coke precursors within zeolite pores. At any conversion level and at any temperature the anisole/cresols ratio is systematically lower for the larger crystal size zeolite, since the secondary transformations of anisole to cresols, by both *intra*-molecular rearrangement and *inter*-molecular alkylation of phenol, is favoured by the longer residence time of anisole within the zeolite pores.

KEYWORDS

Methylation of phenol; Zeolite beta; Crystal size; Surface acidity; FT-IR; Microcalorimetry; *Ab initio* modelling; Catalyst activity and deactivation.

* Corresponding author: Fax +39-02-50314300, E-mail: lucio.forni@unimi.it

1. INTRODUCTION

Methylation of phenol over acidic catalysts represents an industrially interesting process, by which a set of important chemicals and chemical intermediates, such as cresols, anisole and poly-alkylated phenols can be prepared [1]. The most investigated catalysts include strong Brønsted-type acid materials, such as H-Y and H-ZSM5 zeolites [2-13], and weaker acid catalysts as well, such as metal phosphates [14,15]. The main limit of zeolites is the low selectivity achieved to one specific compound, since several products are obtained (*O*-alkylated, mono- and poly-*C*-alkylated), the selectivity of which is a function of phenol conversion, reaction conditions and zeolites characteristics. This is not the case for the heterogeneous basic-catalyzed methylation, which is a much more specific reaction. In fact, it almost exclusively yields the products of ortho-*C*-alkylation [16-20].

Furthermore, alkylation reactions over solid acid catalysts, especially with reactants in gaseous phase, usually are accompanied by several unwanted side reactions, triggered by the same surface acidity of the catalyst, leading to a more or less rapid deactivation of the catalyst, due to fouling by carbonaceous deposits, usually referred to as “coke” [21]. However, it is worth noting that, to the best of our knowledge, the scientific literature on the alkylation with alcohols of phenol and of phenol derivatives, especially from the reaction kinetics point of view, does not take into consideration explicitly any catalyst deactivation effect.

The literature on gas-phase alkylation of phenol with alcohols over Beta zeolites is scarce [22-27]. Over Beta zeolite a somewhat different acidity can add to that based on Al^{3+} sites. Indeed, in such a zeolite randomly intergrown structures of two or even three different polymorphs, with a considerable amount of random stacking faults, leads to a substantial increase of lattice defects and structural disorder [28]. This disorder creates

additional internal surface hydroxylated species (SiOH nests of variable geometrical arrangement) and Lewis-type (L) electron acceptor sites. As a consequence, both catalyst activity and resistance to coking are simultaneously affected by all these features, namely zeolite crystal structure and pore width, nature and concentration of surface acid sites and zeolite crystal size [29-31].

The aim of the present work was to investigate the effect on catalytic performance for phenol methylation of properly prepared samples of H-Beta zeolite of similar Si/Al ratio, but much different crystal size. In fact, it is expected that in a complex reaction pattern, including parallel and consecutive reactions, the distribution of products can be greatly affected by the intra-particle residence time of products. Besides reaction rate and selectivity to the various products, the present analysis takes into account the activity decay and the change of selectivity with time-on-stream, looking for correlations between catalytic behaviour and the zeolites physical-chemical characteristics.

2. EXPERIMENTAL

2.1. Catalyst preparation

Three main samples of Beta zeolite, named beta-1, beta-2 e beta-3, were prepared by hydrothermal synthesis [32,33]. Tetraethyl-orthosilicate (TEOS, 98% pure, Aldrich), tetraethylammonium hydroxide (TEAOH, 40% aqueous solution, Fluka), sodium aluminate (56% Al_2O_3, 37% Na_2O, Carlo Erba) and NaOH (97% pure, Aldrich) were used as reagents. The silico-aluminate precursor gel was obtained by vigorously stirring the mixture of reagents at room temperature for several hours. After the complete hydrolysis of the organo-silicon compound, stirring was further continued for at least 24 h with final gentle warming, to remove the ethanol released.

The synthesis of the zeolite was then carried out at 135ºC (beta-1) or 150ºC (beta-2, beta-3) in PTFE-lined stainless steel autoclaves, tumbling at 20 r.p.m. After 24 h for beta-1, 48 h for beta-2 and 94 h for beta-3 the autoclaves were rapidly cooled and the solid was recovered from the milky suspension by centrifugation at 40,000 *g*. The solid was then repeatedly washed with distilled water till neutrality of the washing liquid, dried at 120ºC overnight and calcined in nitrogen and air flow up to 550ºC, to remove the TEAOH trapped in the channels of the zeolite crystals. The as-prepared samples were then ion-exchanged three times for three hours at 80ºC with fresh 0.1 M ammonium nitrate (Janssen, "pro analysi") solution. After the final exchange, the solid was separated by centrifugation, repeatedly washed with distilled water and calcined in air at 550ºC, to obtain the final protonated zeolite by decomposition of the ammonium ion.

A fourth sample (beta-silicalite, with Si/Al ratio >500) was also prepared for characterisation comparison purposes only. This required the preparation of the special templating agent 4,4'-trimethylene-bis(N-benzyl,N-methyl-piperidinium)-dihydroxide, the usually employed TEAOH failing in leading to the desired BEA structure for very high Si/Al ratios [34].

Beta-10 was a sample kindly supplied by Polimeri Europa srl and it has been used for comparative characterisation purposes only.

The template solution was prepared as follows: 77 g of 4,4'-trimethylene-bis-(1-methyl-piperidine) (Aldrich, 98+% pure) were dissolved in 103 g of ethanol (Fluka, anhydrous). To this solution 110 g of benzyl bromide (Fluka, 98% pure) were added dropwise under vigorous stirring. The solid dibromide precipitate so formed was repeatedly washed with anhydrous ethanol and dried under flowing nitrogen. The dihydroxide was then obtained from the dibromide by electro-dialysis, by employing an electrolytic cell equipped with an anionic membrane separating the cathodic 0.46 M bromide solution from the anodic 25

wt% aqueous ammonia solution. The final 0.79 M solution of the templating agent was finally obtained by low-temperature removal of excess water.

The synthesis of beta-silicalite was then carried out as previously described, in the absence of sodium aluminate and by substituting the 4,4'-trimethylene-bis(N-benzyl,N-methyl-piperidinium)-dihydroxide for TEAOH.

2.2. Catalyst characterisation

Identification of crystalline structure was accomplished by X-ray diffraction (XRD), by means of a Philips PW 1820 powder diffractometer, operated at 40 kV and 40 mA, with Ni-filtered, Cu-Kα radiation (λ = 1.5418 Å). The BET specific surface area (SSA) was measured by N_2 adsorption-desorption at liquid nitrogen temperature, on a Micromeritics ASAP 2010 instrument. Zeolite crystal size and shape were determined by scanning electron microscopy (SEM), by either a Cambridge Stereoscan 150 or a Leica LEO 1430 instrument. Elemental analysis was performed on a Varian Liberty 200 inductively coupled plasma (ICP) spectrometer.

Catalyst surface acidity was measured by FT-IR spectroscopy, by means of a Perkin-Elmer 1750 Spectrometer. Self-supporting wafers of pure zeolite were first evacuated at 500°C *in vacuo* (residual p = 10^{-6} mbar). Then adsorption of pyridine was done at room temperature, and desorption was carried out by outgassing the sample at 50, 150, 250, 350, 450°C. The FT-IR spectrum was recorded after evacuation at each temperature level.

The reactivity towards CH_3OH, the large-excess reactant of the methylation reaction (*vide infra*), has been investigated also by IR spectroscopy. The interaction between CH_3OH and beta-1, beta-2 and beta-3 catalysts, after pre-activation *in vacuo* (residual p = 10^{-5} Torr) at 773 K, has been analysed at 2 cm^{-1} resolution on a Bruker IFS 66 FT-IR spectrometer, equipped with MCT detector. The samples were pre-evacuated as for the acidity measures (*vide supra*).

The adsorption features of the catalysts have been investigated by contacting (at 303 K) the activated samples with CH_3OH vapour, as well as with H_2O vapour, in order to investigate the hydrophilic/hydrophobic properties of the catalysts. The study was performed by using a heat-flow micro-calorimeter Tian-Calvet type (C80 by Sétaram) connected to a high-vacuum gas-volumetric glass apparatus, equipped with a Ceramicell 0-100 Torr transducer gauge by Varian, following a well established procedure [35-37]. All samples were activated *in vacuo* for 2 h at a residual pressure $p \leq 10^{-5}$ Torr at T = 873 K for H-BEA, and at T = 673 K for the all-silica zeolite. The individual activation temperature was selected according to the indications of IR spectroscopy (spectra not reported for brevity), so to achieve the maximum dehydration of the surface compatible with the stability of the structure and aiming at the maximum density of Lewis and Brønsted acidic sites. CH_3OH and H_2O were distilled in vacuo and outgassed by several freeze-pump-thaw cycles. The adsorption measurements have been performed at least twice on a virgin portion of the same batch of the materials, activated under the same conditions, in order to check the reproducibility of the experiments.

At last, a calculation was made relative to the interaction of CH_3OH and H_2O molecules with a molecular cluster simulating a coordinatively unsaturated framework Al(III) site acting as Lewis (L) acidic site. All calculations have been run at *ab-initio* level using the B3-LYP/6-31+G(d,p) model chemistry [38]. The binding energies (BE) of the probe molecules with the L site have been calculated, and compared to the enthalpy change associated to the adsorption processes on the real systems.

2.3. Catalytic activity tests

Methylation of phenol was carried out in a continuous down-flow tubular reactor, at four different temperatures, ranging from 320 to 450°C, at atmospheric total pressure. An excess of methanol with respect to the stoichiometric requirement for the methylation of

phenol was fed (methanol/phenol feed ratio = 7/1). In fact, due to the strong interaction between phenol and the catalyst, acceptable reaction rates are obtained only when the partial pressure of methanol is much higher than that of phenol. Usually methanol/phenol feeding ratios higher than 5 are used [39] for an analysis of the effect of such a ratio on catalytic performance, so to obtain a phenol conversion higher than 10-20% at T < 400°C. On the other hand, feeding ratios higher than 10 favour the formation of poly-alkylated phenols. Our aim was to investigate the selectivity ratio between *O*- and *C*-alkylated compounds, with minimal formation of poly-alkylated products. Therefore, a methanol/phenol molar ratio of 7/1 was selected as a compromise between these two counteracting effects.

0.6 g of catalyst were loaded. The flow rate of reactants was 60 cm^3/min of gaseous N_2 and $1.75x10^{-3}$ cm^3/min of organic liquid feeding mixture, so to have a value of residence time τ = 0.98 s ($cm^3_{catalyst\ bed}$ s/$cm^3_{overall\ gaseous\ feeding\ flow}$). The reactor temperature was kept to the desired value by an electric furnace surrounding the reactor and governed by a TRC, through a thermocouple placed within the catalyst bed. Reactor effluent analysis was made by means of a Thermo, Focus GC gas chromatograph, equipped with a HP-5 semi-capillary column.

When needed, the catalyst was regenerated *in situ* in flowing air (20 cm^3/min) by increasing temperature by 5°C/min from room temperature up to 300°C, then by 0.83°C/min up to 350°C, 400°C and 450°C. After each temperature step (*i.e.* at 300. 350, 400 and 450°C) temperature was kept constant for 1 h.

2.4. Coke analysis

Samples of aged catalyst, recovered after a few hours on-stream at 390°C, were analysed according to a well-known technique [40], to collect information on the amount and nature of the fouling carbonaceous material (coke). A weighed portion of aged catalyst

was disaggregated in HF (40% aqueous solution) to dissolve the zeolite and to collect the remaining carbonaceous solid particles by filtration and drying. The carbonaceous solid particles were repeatedly leached with small portions of fresh CH_2Cl_2 and then dried and weighed. The leaching CH_2Cl_2 solutions were combined and most of the solvent removed *in vacuo* at room temperature. The concentrated solution of the soluble coke was then analysed by gas chromatography-quadrupolar mass spectrometry (GC-QMS) by an Agilent HP 5973N GC-MS instrument.

Furthermore, on beta-1 and beta-2 aged samples only, the amount of accumulated carbonaceous matter was evaluated also by thermogravimetry in air on a TA TGA 2050 Instrument. The following heating program was followed: 80°C in flowing N_2 for 5 min, heating from 80°C to 550°C (5°/min) in 60 ml/min flowing air and final isothermal step at 550°C for 60 min.

3. RESULTS AND DISCUSSION

3.1.Catalysts characterisation

3.1.1. Crystal phase, surface area, crystal size and Si/Al ratio

Under the synthesis conditions adopted, BEA zeolite was the only crystalline phase obtained. The XRD patterns matched those reported in literature [41-43]. Our BEA samples (Fig.1) were the result of intergrowth of two polymorphs, A and B [43], or even of a third polymorph C [42]. However, our XRD patterns did not allow any reliable quantitative determination of the polymorph distribution.

SSA ranged from 480 to 570 m^2/g (Table 1), typical values for these zeolites. SEM micrographs (Fig.2*a,b,d*) showed that beta-1, beta-2 and beta-silicalite were composed of spheroidal-shaped crystals with a narrow crystal size distribution. The beta-3 crystals

appeared slightly cuboidal-shaped (Fig.2*c*). The average size of particles, determined by direct measurement on properly enlarged micrographs for the various zeolites, is given in Table 1. Total pore volume (V_{pTOT}) and micropore volume (V_{pMicr}) (Table 1), determined from the total gas volume adsorbed at saturation and t-plot data, may give an idea of the crystallinity of our samples.

ICP analysis showed for all samples a similar SiO_2/Al_2O_3 molar ratio (Table 1), except of course for the beta-silicalite. Furthermore, the protonated beta-2 and beta-3 (and mainly beta-silicalite) catalysts were almost Na-free, whereas the beta-1 sample contained a considerable amount of exchangeable Na^+ ions (Table 1).

3.1.2 Reactivity toward CH_3OH from FTIR spectroscopy

All the beta samples are characterized by a very low Al content (Table 1). This, accompanied by the high structural defectivity (*vide supra*) of these zeolites, which is associated with a large abundance of silanols, becomes relevant in the spectroscopic features of their reactivity with CH_3OH. Another important point is the concentration of residual Na^+ species, rather abundant (2.42 wt%, Table 1) in beta-1 sample only.

After activation at 773 K all samples (Fig.3*a*) did not present IR bands over 3750 cm^{-1}, characteristic of the hydroxyl groups bound to extra-framework Al (EFA) and all samples showed a strong maximum at 3740 cm^{-1}, due to nearly isolated silanols. Another common characteristic is the broad tail at lower frequency, extending till 3400 cm^{-1}, indicating the presence of an abundant fraction of interacting hydroxyls. No further specific absorption are evident in beta-1 sample: in particular no bands are recognized in the region where bridging OH groups are expected. This observation is in agreement with the fact that beta-1 sample has mainly Na^+ as counterions. Beta-2 sample was characterised by a broad tailed signal, extending from 3740 to 3400 cm^{-1}, due to H-bound silanols. A second weak maximum is observed at 3580 cm^{-1}, where the band due to bridged B groups (3615 cm^{-1})

is superimposed. The situation is very similar to that observed in beta-3 sample, that shows an even more complex shape of the band in the OH stretching region: peak at 3613 cm^{-1} superimposed to the broad component due to H-bonded silanols (maximum at 3500 cm^{-1}). Also in this case an evaluation of the concentration of bridged B groups is prevented by the mixing with the silanols components.

Figure 3*b* shows the reactivity towards CH_3OH of beta 2 and 3. The data on the Na-rich sample, beta-1, are not reported because they did not show any feature associable with bridging Brønsted acid sites. In particular, after interaction with methanol no specific signals ascribable to strong acid sites was noticed (total absence of A, B and C signals, vide infra). In addition, a considerable reversibility of the interaction of beta-1 with methanol was observed, a behaviour typical of purely siliceous materials. This is very likely due to the saturation by Na^+ ions of the strongest acid sites generated by the framework Al ions.

As demonstrated by Pazè et al. [44], in the presence of molecules like H_2O or CH_3OH with medium to high proton affinity, a zeolite, which is characterized by the presence of high Brønsted acidity, is able to realize a strong H-bond interaction, which produces two main effects: at first the band associated to the OH stretching mode is strongly red-shifted, generating an intense and broad absorption which can be extended until 1000 cm^{-1}, while the band due to the overtone of the bending mode of the same species is deeply blue-shifted. From a theoretical point of view, the phenomenon is called Fermi Resonance and the effect on the spectra is the appearance of three bands identified as A, B and C, separated by two Evan's windows: the presence and the relative intensity of these three bands indicate the entity of the interaction and consequently the acidity of the material [44-48].

Coming to the effect of increasing dosages of methanol on beta-2 sample (upper left of Fig.3*b*), one may observe the progressive erosion of the OH bands and the growth of a

very broad absorption with a maximum centred at about 3400 cm^{-1}. This absorption extends till the region of framework vibration, suggesting the presence of some species strongly engaged by methanol. However, as these species are only a minor feature with respect to silanols (characterised by a medium-low-strength acidity) we do not observe clearly, the formation of the A, B, C components. Around 3000 cm^{-1}, the C-H stretching vibrations of CH_3OH are superimposed. In particular, the absorptions at 3000 and 2958 cm^{-1} represent asymmetric vibrations, whereas that at 2854 cm^{-1} is associated with symmetric modes of the CH_3 groups. The frequencies are slightly shifted upward, compared to the vibrations of the free molecule. The band at 2916 cm^{-1} is probably due to overtones of the ν (CH_3) bending mode at 1450 cm^{-1}, enhanced by a Fermi resonance effect [49].

The interaction with methanol was not completely reversible on beta-2, as evidenced by the lower-left of Fig.3*b*. In particular, only part of the external silanols are restored, while the majority of the OH groups are unaffected by prolonged outgassing at room temperature. The fact that methanol is still entrapped within the zeolite cavities is evidenced also by the permanence of the bands associated with the C-H vibration modes around 3000 cm^{-1}.

Coming to the data related to the beta-3 sample (upper right of Fig.3*b*), at low methanol loading we can distinguish the A, B, C triad, caused by Fermi resonance of the ν stretching and 2δ and 2γ overtones of bond 1 (Scheme 1).

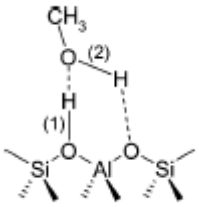

Scheme 1

This in turn induces the formation of two Evans windows, one at about 2720 cm^{-1} and the other at 2000 cm^{-1}. The approximate frequency of the ν (OH) mode of ($_{zeolite}$O-

H…$O_{methanol}$)1 in the absence of Fermi resonance effects can be estimated to 2100 cm^{-1}. The corresponding vibration mode of bond 2 (see Scheme 1) is assigned to a component growing at 3500 cm^{-1}. This band grows in parallel with the A, B, C triplet and confirms the formation of a neutral adduct. The evolution of the spectra in the 2000-1300 cm^{-1} range, where the C component is growing, shows a higher level of complexity. Negative components originate from perturbative effects on the zeolitic framework, inferred by CH_3OH. Moreover, an additional negative band, growing at 1450 cm-1, corresponds to an Evans window, because of the superposition of the C component with $\delta(CH_3)$ mode.

At high methanol coverage the spectra are dominated by an unstructured broad band extending over the entire medium IR region, overshadowing the A, B, C components associated to the formation of the methanol-silanol adducts.

Also with beta-3 the interaction with methanol is only partially reversible, as evidenced by the effect of prolonged outgassing at room temperature (lower right of Fig.3*b*). The last collected spectrum (bold curve) is very similar to what obtained with the beta-2 sample.

It may be concluded that the present materials possess a low concentration of structural ($SiOH^-Al^+$) strong Brønsted acid sites, most of the surface acidity consisting of relatively weaker (SiOH nests) Brønsted silanol species. At reaction temperature the slightly higher abundance of strong acidic sites present in beta-3 sample could play only a minor effect on overall catalytic activity. This acidity distribution can be considered one of the major causes of the relatively lower deactivation rate of high-silica BEA zeolite.

Table 2 gives a summary of the most important IR spectroscopic features of the present samples.

3.1.3. Energetics and hydrophilicity/hydrophobicity of active sites

Energetics of adsorption and hydrophilic/hydrophobic properties of the present catalysts have been investigated, as mentioned, by progressive adsorption of CH_3OH and

water vapour, monitored by micro-calorimetry. Integral heat evolved (Q^{int}), as well as adsorbed amount (n_{ads}) for small adsorptive increments, were determined in the same experiment, following the previously mentioned procedure [35-37]. The reversibility/irreversibility upon room temperature evacuation of first-run-adsorbed phase (ads. I) was checked by performing a second adsorption run (ads. II) after outgassing the sample overnight (residual $p \leq 10^{-5}$ Torr). The adsorbed amounts (n_{ads} = CH_3OH or H_2O molecules per unit cell) were collected as volumetric isotherms. Calorimetric data were collected either as differential heats of adsorption ($q^{diff} = \delta Q^{int}/\delta n_{ads}$), or as integral molar heats of adsorption $[q^{mol}]_p = (Q^{int}/n_{ads})_p$. The $[q^{mol}]_p$ quantities are intrinsically average values, as they refer to the thermal response of the surface as a whole, from the beginning of the adsorption process up to the equilibrium pressure, whereas the q^{diff} quantities represent a reasonable measure of the energy of interaction of the probe molecule with the individual sites, at any adsorbate coverage.

The results for beta-2 and beta-3 samples with CH_3OH as probe are shown in Fig.4. The q^{diff} *vs.* n_{ads} plots give a detailed description of the surface heterogeneity. In particular, the differential heat of adsorption, extrapolated to vanishing coverage (q_0, kJ/mol, Table 1), represents the enthalpy change associated with the adsorption on the most energetic sites. Values of the same order of magnitude have been obtained for the binding energy (BE, kJ/mol) through the *ab initio* calculations (*vide infra*) for the individual molecular probe interaction with the model Lewis acid site and corrected for the basis set superposition error by the standard Boys-Bernardi counterpoise method [50].

By inspecting Fig.4 one may observe that: *i*) The q^{diff} *vs.* n_{ads} experimental points of both beta-2 and beta-3 zeolites are best fitted by the same curve, indicating that no significant difference in the acid strength of the two catalysts can be evidenced by means the room-temperature adsorption of CH_3OH. The curve starts at q_0 ~130 kJ/mol and drops down quite smoothly, eventually approaching the latent heat of liquefaction of CH_3OH (38

kJ/mol) at a coverage corresponding to *ca.*12 molecules adsorbed per unit cell. *ii*) The only detectable differences between the two catalysts is that the CH_3OH adsorption capacity is significantly larger for beta-3 (see inset of Fig.4), the number of molecules adsorbed per unit cell at any equilibrium pressure investigated being higher than for beta-2. We ascribe this difference to the different Si/Al ratio, being the Al content of beta-3 slightly higher than for beta-2, though the two values of Si/Al ratio are too close (130 for the former against 154 for the latter, Table 1) to permit a more detailed comparison. *iii*) The irreversibly adsorbed CH_3OH, evaluated by the difference between the ads. I and ads. II curves, the latter drawn after outgassing overnight the reversibly adsorbed alcohol of ads. I, amounted to *ca*. 20% of the total amount adsorbed by both zeolites. Still, the q^{diff} *vs.* n_{ads} experimental points for the 2^{nd} run were best fitted by the same curve, indicating that neither for reversible adsorption a significant difference between the two catalysts is evidenced by using CH_3OH as molecular probe. *iv*) The quantitative calorimetric data are in agreement with the data from the IR analysis (*vide supra*).

As a preliminary conclusion, beta-2 and beta-3 catalysts show a distribution of acid sites of comparable strength, which abundance is in line (as expected) with Al content, though some effect of materials morphology, and especially of zeolite crystal size, cannot be excluded.

The differential heat of adsorption of H_2O vapour is reported (Fig.5) as a function of the increasing surface coverage (q^{diff} *vs.* n_{ads}) for all the catalysts investigated in the present work. For comparison purposes a Al-free beta-silicalite has been added, together with a previously investigated [35,51] beta-10 sample, characterized by a much higher Al content (Si/Al ≈ 10) *i.e.* by a much higher number of Al atoms per unit cell (~ 6, Table 1). The corresponding volumetric isotherms are shown in the inset. For brevity, in both q^{diff} *vs.* n_{ads} and n_{ads} *vs.* p_{eq} plots only the first-run adsorption data are reported and discussed, but it has been found that in all catalysts (irrespective of the Al content) a fraction of water

molecules was irreversibly adsorbed, whereas for the beta-silicalite the adsorption was found entirely reversible upon room-temperature outgassing. One may observe that: *i)* Initially the experimental data of q^{diff} *vs*. coverage for beta-2 and beta-3 are best fitted by the same curve as for the CH_3OH q^{diff} *vs.* n_{ads} plots (Fig.4), partially confirming the close similarity of the acidic and hydrophilic properties of the two systems. However, the curve starts at q_0 = 160 kJ/mol for the two samples, but drops more rapidly for beta-3 than for beta-2, eventually approaching the latent heat of liquefaction of water (q_L = 44 kJ/mol) at a much lower coverage for beta-3 than for beta-2. Indeed, opposite to methanol, the beta-3 H_2O adsorption capacity is much lower than for beta-2 (see the volumetric isotherms in the inset), indicating that, though the Al content of beta-3 is slightly higher than for beta-2, the population of sites active towards H_2O of the former is lower than that of the latter. In conclusion, the beta-3 zeolite is less hydrophilic than beta-2, in spite of the lower Si/Al ratio, as if the larger crystal size of the former would inhibit the interaction with water. *ii*) The q_0 value (close to 100 kJ/mol) for the Na-rich beta-1 catalyst is much lower than for beta-2 and beta-3, as expected. Furthermore, as far as the coverage increases, the beta-1 curve does merge into the beta-2 curve, according to the closer similarity of the crystal size. It is worth noting that the beta-1 water adsorption capacity (per unit cell) is only slightly lower than for beta-2, and much higher than for beta-3, according to the lower concentration of strong acid sites (see inset of Fig.5). *iii*) The q^{diff} *vs.* n_{ads} plot for beta-silicalite lies below those of the other catalysts in the whole examined range of coverage, in agreement with the absence of strong acidic sites, associated with framework Al species. The q_0 value for this sample is close to 80 kJ/mol, much lower than for other zeolites. It is however worth noticing that the q^{diff} *vs.* n_{ads} plot for beta-silicalite lies above the latent heat of liquefaction of water (q_L = 44 kJ/mol), as typical of an hydrophilic surface [35-37].

By comparing the results obtained for the present-work beta zeolites with those previously obtained by some of us on beta-10, the difference in calorimetric response of the Al-rich beta-10 system is dramatically evident, in that both beta-10 q^{diff} *vs.* n_{ads} and n_{ads} *vs.* p_{eq} plots lie well above the corresponding curves for the present-work beta zeolites. This strongly confirms that the population of strong acidic sites is much more abundant in the beta-10 catalyst, as expected. However, the very initial heat of adsorption of water is quite close for beta-2, beta-3 and beta-10 catalysts (q_0 ~160 kJ/mol in all cases), suggesting that the difference in calorimetric response is connected to the abundance, more than to the strength of acid sites.

The integral molar heat of adsorption q_{mol} (*vide supra*) determined at equilibrium pressure corresponding to either 2 or 4 H_2O molecules/uc coverage are shown in Fig.6 *a* and *b*, respectively, as a function of the crystal size of the investigated materials (see Table 1). Again the beta-10 datum is reported for comparison. It can be noticed that: *i*) The q_{mol} value is very close (~ 85 kJ/mol, irrespective of the crystal size), for all the present catalysts, characterized by a close Si/Al ratio (130 < Si/Al < 154). *ii*) The q_{mol} value for beta-silicalite is lower (~ 50 kJ/mol), according to the fact that in this case only H-bonding interactions, much less energetic than both the Lewis and Brønsted acid-base interactions, are operative. *iii*) The q_{mol} value for beta-10 is much higher (~ 160 kJ/mol), since a coverage of 2 H_2O molecules/unit cell is still very low (only one third of acidic sites associated to framework Al have already reacted). *iv*) At 4 H_2O molecules/unit cell coverage, over beta-10 a few strong acidic sites remain still available, but in this case the q_{mol} values (which are intrinsically average values, including all interactions contributions) are much closer (~ 100 kJ/mol) to the q_{mol} values (~ 75 kJ/mol) for the beta-1-2-3 catalysts. *v*) At high coverage the difference between the beta-1-2-3 set and beta-silicalite is much smaller, according to the fact that at such a coverage also in the beta-1-2-3 catalysts the

interaction is dominated by H-bonding (on both silanols and already adsorbed water molecules).

Fig.7 shows the B3LYP/6-31+G(d,p) optimized structures of the clusters adopted to mimic the L acid site interacting with the CH_3OH (a) and H_2O (b) molecule. The calculated binding energies (BE) are 125 and 110 kJ/mol, respectively. These values are in agreement with the calorimetric energetic data (differential heats of adsorption) measured in the early stage of the process and suggest that at least a fraction of acid sites is likely Lewis in nature.

3.1.4. Nature and strength of surface acid sites

Fig.s 8 and 9 show the FT-IR spectra recorded after pyridine adsorption at room temperature, followed by desorption at increasing temperatures, for samples beta-1 and beta-2, respectively. In the case of beta-1 (Fig.8) the intensity of the band associated to pyridinium cation (1546 cm-1) is nil, that relative to the interaction with Lewis sites (1455 cm^{-1}) is very weak, and pyridine is totally released already after evacuation at 250°C. Finally, the amount of pyridine interacting with silanols (bands at 1446 and 1596 cm^{-1}) [52] is lower than in beta-2 catalysts (Fig.9). In beta-1, silanols are clearly the only sites present in non-negligible amount.

In the case of beta-2 (Fig.9), the strong bands at 1446 and 1596 cm^{-1}, due to pyridine adsorbed on silanols, progressively decrease when increasing temperature and totally disappear after evacuation at 250°C. By contrast, some pyridine adsorbed on Lewis sites (1455 cm^{-1}) remains even after evacuation at 450°C. This indicates the presence of strong Lewis-type acid sites, in line with what found by the other techniques. The band at 1546 cm^{-1}, due to the interaction with Brønsted sites, is very weak, as expected from the low concentration of these sites in high-silica zeolites. When the sample is heated, the intensity first increases, likely due to the evolution of the hydrogen bonding with the –OH

group into pyridinium ions, and then decreases; totally disappearing after evacuation at 450°C. The spectra recorded with beta-3 samples (not reported for brevity) were very similar to those of beta-2.

3.2. Catalyst activity and deactivation rate

There is a wide literature dealing with the use of zeolites as catalysts for the liquid-phase and gas-phase methylation of phenol. With MFI zeolites, at temperature higher than 350°C Kaliaguine et al. [2,53] found that the reaction leads to a variety of products, amongst which the most relevant were cresols and xylenols. A mechanism was proposed in which diphenyl ether and anisole (the two products of etherification) are the reaction intermediates and interact with Brønsted sites and carbonium ions to yield *C*-methylated products. The reaction pattern was confirmed by others [12], who also found that in liquid-phase methylation anisole and cresols are primary products and that anisole undergoes consecutive transformation to cresols.

With H-Y zeolites, at 200°C and phenol conversion lower than 15% *O*-alkylation was found to be quicker than *C*-alkylation (the two reactions were substantially parallel), with *o*-/*p*-cresol molar ratio equal to 1.5. Anisole disproportioned into phenol and methyl-anisoles, whereas direct isomerisation of anisole into cresols did not occur. Anisole also acted as an alkylating agent for phenol, to yield cresols and methyl-anisoles. The latter reaction was favoured over the disproportion of anisole in the presence of phenol [5]. An important contribution to *C*-alkylated compounds also derived from the intra-molecular rearrangement of anisole into *o*-cresol [9]. The exchange of protons with Na or the poisoning with NH_3 led to an increase of the anisole/cresols ratio, indicating that anisole formation required sites with lower acid strength as compared to those needed for cresol formation [6], in agreement with what proposed formerly by Namba et al [10]. Similar results were obtained by other authors [7-9].

The reactivity of Al-MCM-41 also is imilar to that of H-Y [39], with anisole acting as a reaction intermediate. The mechanism of reaction, involving the direct formation of anisole and cresols and the consecutive transformation of anisole, was recently confirmed by means of *in-situ* measurements by Weitkamp *et al*. [54].

With Beta zeolites, again the formation of anisole and cresols occurred through parallel reactions [22,23]. Anisole then was the intermediate in the formation of cresols. As for the effect of the Si/Al ratio, higher ratios implied a lower phenol conversion and hence a greater selectivity to anisole. No effect of shape-selectivity was found.

As for the electrophylic substitution on phenol, the active species is generated by adsorption of methanol and formation of framework-bound methoxonium ($CH_3OH_2^+$) ion and methoxy species, which can coexist at low temperature. However, at higher temperature the equilibrium is shifted towards the methoxy species [55], which acts as the electrophylic alkylating agent on alkylaromatics [56,57].

3.2.1. Performance of beta-2 and beta-3 catalysts in phenol methylation

The effect of time-on-stream on conversion of phenol in methylation over the beta-2 catalyst, at four different temperatures, is reported in Fig.10, whereas Fig.11 shows the corresponding distribution of products, as measured at 450°C. The following considerations are of relevance: *i*) There is a considerable deactivation of catalyst with increasing time-on-stream. *ii*) Initial conversion is 100% at temperature higher than 320°C, whereas it approaches 75% at 320°C. *iii*) Deactivation rate appears substantially independent of temperature. *iv*) Deactivation is accompanied by a change in the relative amount of products. Specifically, at total conversion the main products are poly-alkylated compounds (mainly di- and tri-methyl phenols and methyl and di-methyl anisoles), whereas the progressive decrease of conversion leads to a rapid decrease of the latter compounds, with a corresponding increase of primary alkylation products: anisole, *o*-cresol

and *p*-cresol. Amongst the latter, the prevailing one is *o*-cresol. *v*) A more detailed investigation of the trend of products formation indicates that the selectivity to cresols decreases monotonously when conversion increases, whereas the selectivity to anisole decreases more rapidly. This is because the cresols undergo consecutive reactions of transformation to diphenols, whereas anisole not only undergoes the analogous consecutive alkylation to methyl-anisole, but also it acts as an alkylating agent by itself. Indeed, it is known that anisole can either rearrange to *o*-cresol (*intra*-molecular rearrangement) or act as an *inter*-molecular alkylating agent, with co-generation of phenol [5,9,39,54]. *vi*) At lower temperatures the distribution of products is similar to that obtained at 450°C. The only difference is the selectivity ratio between anisole and cresols.

It is worth noting that in the alkylation of alkylbenzenes (*e.g.*, of toluene) with methanol it is possible to obtain a high selectivity to the *para*-*C*-alkylated compound. By contrast, in the alkylation of activated arenes, such as phenol, diphenols and aniline, with olefins or with alcohols, the selectivity for the *para*-electrophilic substitution is lower than expected [58]. Indeed, on amorphous acid catalysts, the selectivity to *o*-cresol can even approach 100% [8,59,60]. The low selectivity to *p*-cresol in phenol methylation has been attributed to different reasons [61,62] and specifically: *i*) The alkylation at heteroatom is an intermediate step in *C*-alkylation by the olefin or by the alcohol [63]. *ii*) An interaction exists between the alkylating agent and the oxygen atom of phenol, which favours the alkylation at the *ortho* position [5,63]. *iii*) A reaction between adsorbed anisole, which acts as the alkylating agent, and gas-phase phenol can be hypothesised [8], in which the interaction between the two O atoms puts the methyl group of anisole closer to the *ortho* position of phenol. *iv*) Furthermore, even in the homogeneous acid-catalysed electrophylic substitution on phenols, usually *ortho*/*para* ratios higher than the statistic value 2/1 are found [58,64]. This implies that adsorptive/geometric effects are not the main reason for the regioselectivity observed.

So, the overall mechanism for the acid-catalysed methylation of phenol [8] includes the direct *C*-alkylation at the *ortho* and *para* positions (in confined environments the direct *para*-*C*-alkylation can be preferred) and the *O*-alkylation to yield anisole, the ratio *C*-/*O*-alkylation being a function of the catalyst acid strength. The secondary, consecutive *intra*-molecular rearrangement of anisole to *o*-cresol makes the final *ortho*/*para*-*C*-alkylation ratio to become very high, especially over less acidic catalysts (*e.g.*, on amorphous materials).

The performance of the beta-3 catalyst is summarized in Fig.12 (effect of time-on-stream on conversion of phenol, at four temperatures) and Fig.13 (effect of time-on-stream on distribution of reaction products, at 450°C). The comparison with the data obtained with beta-2 zeolite (Fig.10 and 11) highlights that: *i*) The initial activity of the beta-3 zeolite is greater than that of beta-2. This is evident for the runs at 320°C only, since higher temperatures lead to total or almost total conversion for both catalysts. This difference is very likely due to the higher *intra*-particle residence time of reactants in the larger crystal size zeolite. *ii*) At higher temperatures the deactivation rate seems not much affected by crystal size. Only at 320 and 350°C the beta-2 zeolite seems to exhibit a quicker deactivation rate than beta-3. This is likely due to the shorter mean path within smaller zeolite crystals, whose pores become obstructed more quickly than the longer pores of beta-3. Since the difference is evident at low temperature only, this means that the species responsible for deactivation are not the alkyl-aromatics formed by methanol transformation (the formation of which is favoured at high temperature), but more likely phenol and oxygenated products, the diffusion of which is slower at lower temperature, due to their low volatility and to their stronger interaction with the zeolite acid sites. The characterisation of spent catalysts (*vide supra*) confirm this hypothesis. *iii*) The nature of products and the effect of conversion and of temperature on selectivity do not differ significantly from those observed with beta-2 catalyst.

At last, Fig.14 shows the effect of phenol conversion on the anisole/cresols ratio at 320, 390 and 450°C on beta-2 and beta-3 catalysts. One may see that: *i*) The ratio decreases with increasing conversion, due to the secondary, consecutive transformations occurring on anisole, with formation of additional cresols; *ii*) The ratio decreases when increasing temperature at any conversion level, showing that low temperature favours the primary methylation at oxygen (and hence to anisole), with respect to the primary methylation at aromatic carbons.

Even though the comparison between zeolites is arguable when done under conditions that lead to catalyst deactivation and coke accumulation, nevertheless the data of Fig. 14 indicate that the anisole/cresols ratio with beta-3 zeolite is systematically lower than for beta-2 at any conversion level and at any temperature. This means that the extent of the consecutive transformation of anisole to cresols is higher in the larger crystal size zeolite, as a consequence of the longer permanence of anisole within the zeolite pores, favouring both the secondary, consecutive *intra*-molecular rearrangement and *inter*-molecular alkylation of anisole.

An effect of crystal size on products distribution was also reported by Moon et al for phenol methylation over MCM-22 [12]. The authors found that *p*-cresol formed preferentially with respect to *o*-cresol, especially in the case of catalysts where the zeolite crystal sizes were greater than 1 μm. It was thus proposed that in the case of MCM-22 the 10MR pores allow easy diffusion of *p*-cresol and that the effect of this phenomenon is enhanced when the crystal size is relatively large. Also in the case of cresols isomerisation, the distribution of isomers (the formation of which occurs both by intramolecular methyl shift and bimolecular disproportionation) was governed by product desorption/diffusion. Shape selectivity favoured monomolecular reactions [65].

3.2.2. Transformation of methanol into poly-alkylated benzenes

During reaction with phenol, methanol also undergoes a parallel transformation to olefins and alkylbenzenes. The relative amount of the two classes of compounds is a function of the reaction temperature, higher temperatures favouring the formation of the latter compounds. Therefore, we also investigated the formation of alkylbenzenes. The yield to these compounds is shown in Fig.s 15 and 16, for the beta-2 and beta-3 catalysts, respectively, as a function of time-on-stream at 450°C. The same Figures also report the conversion of methanol, which also includes the amount converted for phenol methylation. It is worth noting that no “light” products of methanol decomposition (*i.e*. CO, CO_2, H_2) formed.

The principal products coming from methanol transformation were toluene, pentamethylbenzene and hexamethylbenzene. The yield to these compounds was relevant and the greater fraction of methanol was converted to poly-alkylated benzenes, rather than being involved in phenol methylation. This aspect has never been reported in the literature dealing with the gas-phase methylation of phenol catalysed by zeolites. Furthermore, it is evident that this is one reason for the need of feeding a large excess of methanol with respect to the stoichiometric requirement for the mono-alkyation of phenol. The competitive reaction of methanol transformation to alkylbenzenes makes the amount of methanol available for phenol methylation to become very low.

The conversion of methanol increased during the elapsing reaction time, due to the increased formation of poly-alkylated compounds, whereas, at the opposite, the amount of methanol that reacts with phenol decreased (see Figs. 10 and 12). Therefore, it seems that the active sites for the formation of these compounds are generated during reaction, while the sites responsible for the generation of the active species for the electrophilic substitution at the phenol ring are progressively poisoned. This clearly indicates that the mechanism of the two reactions is different. The conversion of methanol reached a maximum at approximately 800-1000 minutes-on-stream, after which it rapidly fell down,

likely because of the considerable amount of coke accumulated in the catalyst, due to the growth of poly-nuclear aromatics.

The behaviour of the two zeolites was not much different, a part from the slightly different value of time-on-stream at which the maximum methanol conversion was attained (700 min for beta-2, against 1000 min for beta-3). This is probably due to the larger crystal size of the latter sample, that made pore filling by coke to take longer time than with the former sample. With both samples the yield to toluene decreased, whereas that to pentamethylbenzene showed a maximum before the reaction time needed to reach the highest methanol conversion. The yield to the totally alkylated compound (hexamethylbenzene) increased, until the maximum methanol conversion was reached. This indicates that the growth of the molecular weight occurred in a consecutive-steps network fashion.

The mechanism for the formation of alkylated benzenes by self-reaction of methanol over zeolites (the MTG process) includes one first step of dehydration of methanol to dimethylether. Two mechanisms have been proposed, either an indirect pathway, in which the adsorbed methanol reacts with the methoxy species, which then reacts with another methanol molecule to dimethylether [66], or the direct pathway, in which two methanol molecules react over an acid site, with the formation of dimethylether and H_2O in one step [67]. The surface methoxy species $SiO(CH_3)Al$ has been demonstrated to play a role in the formation of dimethylether [68]. The further conversion of the equilibrium mixture of methanol and dimethylether (and water as well) is dominated by a “hydrocarbon pool” route [69,70], in which methanol is directly added onto reactive organic compounds to form aliphatic and aromatic hydrocarbons. The methoxy species also plays a role in the kinetic “induction period”, leading to the reactive hydrocarbon pool.

Alternative “direct” mechanisms have been proposed, in which either a carbenium ion (CH_3^+) reacts with dimethylether to generate either a carbonium ion (CH_3-CH_3^+-OCH_3), or

an oxonium ylide species. Other mechanisms include a carbene species (:CH_2) as the reaction intermediate (see the review by Haw *et al*. [71] for an analysis of the several mechanisms proposed in literature). The methoxy species acts as an alkylating agent in the presence of aromatic compounds. Furthermore, at T > 170°C, hydrogen atoms are abstracted by basic oxygen atoms of the framework, with formation of surface-stabilized intermediates of ylide or carbene nature [72], which are responsible for the methylation of aliphatic compounds, and for the formation of hydrocarbons, both aliphatic and aromatic (polymethylbenzenes) [73].

In the case of Beta zeolites, the predominant aromatic compounds in methanol transformation at high T are hexamethylbenzenes and pentamethylbenzenes (in full agreement with our results), while ZSM-5 gave mostly dimethyl and trimethylbenzenes [74]. These compounds can be further converted to naphthalene derivatives, which are finally responsible for the formation of coke precursors and of zeolite deactivation [21].

Our data support the need for an induction period for the formation of these compounds, associated to the generation of a “hydrocarbon pool”. This corresponds to the progressive increase of methanol transformation into poly-alkyl benzenes shown in Fig.s 15 and 16. The progressive transformation of the hydrocarbon pool into heavier and heavier poly-alkylated compounds and to coke eventually leads to the complete deactivation of the catalyst.

3.2.3. Coke composition

Thermogravimetric (TG) analysis showed that the weight loss due to burning out of coke components by calcination in air amounted to 3.4%, while for beta-2 it was considerably higher, 12.8%. This obviously relates to the higher acidity of beta-2 as compared to beta-1. The organic matter extracted from beta-2 with CH_2Cl_2 amounted to 12.7%, perfectly in line with the value determined by TG. The GC-QMS analysis of the

extracted fraction showed the presence of the following compounds: phenol (8 mol%), *o*- and *p*-cresols (4%), dimethyl-phenols (8%), trimethyl-phenols (15%), tetramethy-phenols (18%), pentamethyl-benzene (5%), hexamethyl-benzene (5%), 3-ethyl-5-methyl-phenol (1%), 2-hydroxyphenyl-phenylmethanone (15%), 2-methyl-5-(1-methylethyl)-phenol (6%), 1-methoxy-4-methyl-2-(1-methylethyl)-benzene (15%). In the case of beta-1, instead, the following compounds were identified: phenol, cresols, dimethyl-phenols, trimethyl-phenols, tetramethyl-phenols and (dimethyl-ethyl)-phenols. Therefore, with the latter catalyst there was substantially no formation of poly-alkylbenzenes, *i.e.* the species coming from the transformation of methanol. With both catalysts, the insoluble coke recovered after dissolution of the zeolite was almost weightless and presumably composed of high-MW polynuclear species, their very low amount preventing however any reliable quantitative determination.

Therefore, these data indicate that the presence of strong acid sites in beta-2 is responsible for the formation of poly-alkylbenzenes, while silanols (present in both beta-1 and beta-2 samples, though in lower concentration in the former catalyst) are strong enough to catalyse the reaction of phenol methylation. This also indicates that the active methanol species able to attack phenol to yield methylated phenol is different from the species self-reacting to yield poly-alkylbenzenes. Indeed, on one hand the latter species can form only on acid sites much stronger than those required to form the former. On the other hand, the former species, though being not able to generate poly-alkylbenzenes, is electrophylic enough to react with phenol.

Furthermore, beta-1 was less active than beta-2 and beta-3, but did exhibit a deactivation rate comparable to that of the latter catalysts. This indicates that the main reason for catalyst deactivation in phenol methylation is associated to the build-up in catalyst pores of oxygen-containing species (phenol and alkylated phenol compounds). It is worth noting that the analysis of the compounds retained in the pores showed a high

concentration of heavier compounds (poly-alkylated phenol), that instead are present in low concentration in the reactors' outcoming products stream. Therefore, heavier phenol derivatives are the species that more accumulate in the porous structure, as expected, due to their more cumbersome structure.

Therefore, two different deactivation mechanisms can be envisaged. One mechanism, responsible for the progressive deactivation of the catalyst in the methylation of phenol, is due to the retention of heavy, oxygenated compounds (*i.e.*, poly-alkylated phenols). This derives from the strong interaction of phenol and phenol derivatives with the active sites, which establishes from the very beginning of the reaction and hinders the generation of the active species responsible for the electrophylic attack to the phenol aromatic ring. Despite this, methanol conversion progressively increases during the first hours-on-stream, due to the fact that methanol is simultaneously converted to alkyl and poly-alkyl benzenes, generated from the building up of the "hydrocarbon pool" inside pores. This is supported also by the change in the nature of the alkyl benzenes forming along with increasing methanol conversion. However, the progressive hardening of these species generates poly-nuclear aromatics, which in a few hours fills up the pores and eventually deactivates the catalyst.

CONCLUSIONS

The systematic analysis carried out in the present work allowed to throw light on several aspects of the methylation of phenol, from many points of view, ranging from catalyst structure, crystal size and surface acidity characteristics, to energetics of interaction between methanol (and water) and acid sites, to the effect of all these characteristics on kinetics and on mechanistic features of the catalytic reaction and of

catalyst deactivation phenomena. The main conclusions one can draw from the present results are the following:

1. High Si/Al ratio BEA-structured zeolite in protonated form is a very active catalyst for the methylation of phenol, leading to cresols and anisole as primary products, which rapidly methylate to poly-alkylated phenols. As deactivation proceeds, the selectivity to cresols and anisole increases substantially, together with a rapid decrease of selectivity to poly-alkylated species.
2. In this protonated zeolite acidity is prevalently of Brønsted type, independently of zeolite crystal size. However, the main part of the acid sites are of medium-to-low-strength. Indeed, high-strength Lewis-type sites are either almost absent, especially when metal cations partially substitute for protons, or seem to play a role prevalently in catalyst deactivation.
3. Stacking faults in the zeolite framework, generated by the intergrowth of at least two BEA polymorphs, can increase the concentration of relatively low-strength silanols-based acid sites, which seem however sufficiently active to trigger the phenol methylation primary reaction.
4. Deactivation is originated essentially by phenol and poly-alkylated phenol-derivatives. Self oligomerisation-cyclisation of methanol to olefins and aromatics, followed by further alkylation to aromatic C atoms, contributes more significantly to catalyst deactivation only for time-on stream values longer than a few hours.
5. At higher temperature all the zeolites deactivate at a comparable rate, whereas at lower temperature initial catalytic activity is higher for larger crystal size zeolite, due to the longer diffusion time of reactants within longer zeolite pores, favouring a longer contact with active sites.
6. At any conversion level and at any temperature the anisole/cresols ratio is systematically lower for the larger crystal size zeolite, since the secondary

transformations of anisole to cresols by both *intra*-molecular rearrangement and *inter*-molecular alkylation of phenol is favoured by the longer residence time of anisole within the zeolite pores.

REFERENCES

1. Ullmann's Encyclopedia of Industrial Chemistry, 6th Edition, Wiley-VCH, Weinheim (2003), Vol.9, p.642
2. P.D. Chantal, S. Kaliaguine, J.L. Grandmaison, Appl. Catal., 18 (1985) 133
3. R. Pierantozzi, A.F. Nordquist, Appl. Catal., 21 (1986) 263
4. S.C. Lee, S.W. Lee, K.S. Kim, T.J. Lee, D.H. Kim, J.Chang Kim, Catal. Today, 44 (1998) 253
5. M. Marczewski, J.-P. Bodibo, G. Perot, M. Guisnet, J. Molec. Catal., 50 (1989) 211
6. L. Garcia, G. Giannetto, M.R. Goldwasser, M. Guisnet, P. Magnoux, Catal. Lett., 37 (1996) 121
7. S. Balsamà, P. Beltrame, P.L. Beltrame, P. Carniti, L. Forni, G. Zuretti, Appl. Catal., 13 (1984) 161
8. P. Beltrame, P.L. Beltrame, P. Carniti, A. Castelli, L. Forni, Appl. Catal., 29 (1987) 327
9. R.F. Parton, J.M. Jacobs, H. van Ooteghem, P.A. Jacobs, Stud. Surf. Sci. Catal., 46 (1989) 211
10. S. Namba, T. Yashima, Y. Itaba, N. Hara, Stud. Surf. Sci. Catal., 5 (1980) 105
11. Z.-H. Fu, Y. Ono, Catal. Lett., 21 (1993) 43
12. G. Moon, W. Böhringer, C.T. O'Connor, Catal. Today, 97 (2004) 291
13. M.D. Romero, G. Ovejero, A. Rodriguez, J.M. Gomez, I. Agueda, Ind. Eng. Chem. Res., 43 (2004) 8194
14. G. Sarala Devi, D. Giridhar, B.M. Reddy, J. Molec. Catal., 181 (2002) 173
15. F.M. Bautista, J.M. Campelo, A. Garcia, D. Luna, J.M. Marinas, A. Romero, J.A. Navio and M. Macias, Appl. Catal., A, 99 (1993) 161
16. R. Bal, B.B. Tope, S. Sivasanker, J. Mol. Catal. A, 181 (2002) 161
17. S. Velu, C.S. Swamy, Appl. Catal. A, 145 (1996) 141
18. V.V. Rao, V.Durgakumari, S. Narayanan, Appl. Catal., 49 (1989) 165
19. S. Velu, C.S. Swamy, Appl. Catal. A, 162 (1997) 81

20. M. Bolognini, F. Cavani, D. Scagliarini, C. Flego, C. Perego, M. Saba, Catal. Today, 75 (2002) 103
21. M. Bjørgen, U. Olsbye, S. Kolboe, J. Catal., 215 (2003) 30
22. J. Xu, A.-Z. Yan, Q.-H. Xu, React. Kinet. Catal. Lett., 62 (1997) 71
23. G. Chen, X. Liu, Chin. J. Catal., 19 (1998) 427
24. K. K. Cheralathan, I. S. Kumar, M. Palanichamy, V. Murugesan, Appl. Catal. A, 241 (2003) 247
25. A. V. Krishnan, K. Ojha, and N. C. Pradhan, Org. Proc. Res. Dev., 6 (2002) 132
26. K. Zhang, C. Huang, H. Zhang, S. Xiang, S. Liu, D. Xu, H. Li, Appl. Catal. A, 166 (1998) 89
27. E. Dumitriu, V. Hulea, J. Catal., 218 (2003) 249
28. I.Kiricsi, C.Flego, G.Pazzuconi, W.O.Parker, Jr., R.Millini, C.Perego, G.Bellussi, J.Phys.Chem., 98 (1994) 4627
29. G.Bellussi, G.Pazzuconi, C.Perego, G.Girotti, G.Terzoni, J.Catal., 157 (1995) 227
30. G.Perego, S.Amarilli, R.Millini, G.Bellussi, G.Girotti, G.Terzoni, Mesop. Mater., 6 (1996) 395
31. G.Girotti, EurpaCat-IV, Rimini, Sept. 5-10, 1997, Book of Abstracts, KN11
32. J. Pérez-Pariente et al., Appl. Catal., 31 (1987) 35
33. M.A. Camblor, J. Pérez-Pariente, Zeolites, 11 (1991) 202
34. U.S. Patent 5,453,511, Sept. 26,1995
35. V. Bolis, B. Fubini, L. Marchese, G. Martra, D. Costa, J.Chem.Soc., Faraday Trans. 1991, 87, 497
36. V. Bolis, A. Cavenago, B. Fubini, Langmuir 1997, 13, 895
37. V. Bolis, C. Busco, S. Bordiga, P. Ugliengo, C. Lamberti, A. Zecchina, Appl. Surf. Sci. 2002, 196, 56
38. V. Bolis, C. Busco, P. Ugliengo, J. Phys. Chem. B, in press
39. K. G. Bhattacharyya, A.K. Talukdar, P. Das, S. Sivasanker, J. Molec. Catal. A, 197 (2003) 255
40. P. Magnoux, P. Roger, C. Canaff, V. Fouché, N.S. Gnep, M. Guisnet, Stud. Surf. Sci. Catal., 34 (1987) 317
41. R.L. Wadlinger, G.T. Kerr, E.J. Rosinski, U.S. Patent 3,308,069 (1967) and reissued U.S. Pat. Re 28,431 (1975) assigned to Mobil Oil Corp
42. J.M. Newsam, M.M.J. Treacy, W.T. Koetsier, C. De Gruyter, Proc. R. Soc. London A, 420 (1988) 375

43. J.B. Higgins, R.B. La Pierre, J.L. Schlenker, A.C. Rohrman, J.D. Wood, G.T. Kerr, W.J. Rohrbaugh, Zeolites, 8 (1988) 446
44. C. Pazè, S. Bordiga, C. Lamberti, M. Salvalaggio, A. Zecchina, J. Phys. Chem. B 101, (1997) 4740-4751.
45. A. Zecchina, S. Bordiga, G. Spoto, D. Scarano, G. Spanò, F. Geobaldo, J. Chem. Soc., Faraday Trans., 9 (1996) 4863-4875.
46. S. Bordiga S., L. Regli, D. Cocina, C. Lamberti, C. M. Bjørgen, K.P. Lillerud, J. Phys. Chem. B, 109, (2005) 2779-2784
47. G.Herzberg, Molecular Spectra and Molecular Structure, F. R. S.-II. Infrared and Raman Spectra of Polyatomic Molecules; D. Van Nostrand Company, Inc.: New York, 1945; p 216.
48. S. E. Odinokov, A. V. Jogansen, Spetrochim. Acta, Part A, 28 (1972) 2343-2350.
49. N. B. Coltup, L. H.; Daly, S. E Wiberley, Introduction to infrared and Raman Spectroscopy; Academic Press: London, 1995; p 220.
50. S. F. Boys, F. Bernardi, Mol. Phys. 1970, 553
51. V. Bolis, M. Broyer, A. Barbaglia, C. Busco, G. M. Foddanu, P. Ugliengo, J. Molec. Catal., A: Chemical, 204 (2003), 561
52. G. Busca, Phys. Chem. Chem. Phys. 1 (1999) 723.
53. M. Renaud, P.D. Chantal, S. Kaliaguine, Canad. J. Chem. Eng., 64 (1986) 787
54. W. Wang, P. L. De Cola, R. Glaeser, I.I. Ivanova, J. Weitkamp, M. Hunger, Catal. Lett 94 (2004) 119
55. J. Rakoczy, T. Romotowski, Zeolites, 13 (1993) 256
56. G. Mirth, J. Lercher, J. Catal., 132 (1991) 244
57. A. Corma, G. Sastre, P.M. Viruela, J. Mol. Catal. A, 100 (1995) 75
58. R.F. Parton, J.M. Jacobs, D.R. Huybrechts, P.A. Jacobs, Stud. Surf. Sci. Catal., 46 (1989) 163, and references therein
59. J.M. Campelo, A. Garcia, D. Luna, J.M. Marinas, M.S. Moreno, Stud. Surf. Sci. Catal., 41 (1988) 249
60. J.M. Campelo, A. Garcia, D. Luna, J.M. Marinas, M.S. Moreno, Bull. Soc. Chim. France, 2 (1988) 283
61. P. Espeel, R. Parton, H. Toufar, J. Martens, W. Hölderich, P. Jacobs, in “Catalysis and Zeolites. Fundamentals and Applications”, J. Weitkamp and L. Puppe (Eds.), Springer, Berlin, 1999, Ch. 6, p.377
62. J.B. Moffat, Catal. Rev. Sci. Eng., 18 (1978) 199

63. M. Marczewski, G. Perot, M. Guisnet, Stud. Surf. Sci. Catal., 41 (1988) 273
64. Patai “The Chemistry of the Hydroxyl Group”, Interscience Publ. John Wiley & Sons, (1971) 414
65. F.E. Imbert, M. Guisnet, F. Gnep, J. Catal., 195 (2000) 279
66. T.R. Forester, R.F. Howe, J. Am. Chem. Soc., 109 (1987) 5076
67. J. Bandiera, C. Naccache, Appl. Catal., 69 (1991) 139
68. W. Wang, M. Seiler, M. Hunger, J. Phys. Chem. B, 105 (2001) 12553
69. I.M. Dahl, S. Kolboe, J. Catal., 149 (1994) 458
70. B. Arstad, S. Kolboe, J. Am. Chem. Soc., 123 (2001) 8137
71. J.F. Haw, W. Song, D.M. Marcus, J.B. Nicholas, Acc. Chem. Res., 26 (2003) 317
72. P.E. Sinclair, C.R.A. Catlow, J. Phys. Chem. B, 101 (1997) 295
73. W. Wang, A. Buchholz, M. Seiler, M. Hunger, J. Am. Chem. Soc., 125 (2003) 15260
74. Ø. Mikkelsen, S. Kolboe, Microp. Mesop. Mater., 29 (1999) 173

ACKNOWLEDGEMENTS

The financial aid of INSTM, through the Prisma 2002 programme is gratefully acknowledged. We are also indebted with dr A.Casalini, Stazione Sperimentale per i Combustibili (S.Donato Milanese) for the GC-QMS analysis of coke.

FIGURE CAPTIONS

Fig.1. XRD patterns of the catalysts prepared. *a,b,c* refer to polymorphs A,B and C (see ref. 42,43).

Fig. 2 SEM micrographs of: (*a*) beta-1; (*b*) beta-2; (*c*) beta-3; (*d*) beta-silicalite

Fig.3. *a*) IR spectra of beta-1, beta-2 and beta-3 zeolites outgassed at 753 K; *b*) IR spectra of beta-2 and beta-3 zeolites (left and right couple of Figures, respectively). Effect of the interaction with CH_3OH. Top parts of the figure report data related to increasing amounts of methanol, Bottom parts of the figures reports the effect of progressive pumping out at room temperature.

Fig.4: Differential heats of adsorption of $CH_3OH_{vap.}$ on beta-2 (•) and beta-3 (▼) zeolites as a function of the increasing coverage (q^{diff} *vs*. n_{ads}). Inset: volumetric isotherms, n_{ads} (CH_3OH molecules/uc) *vs.* p_{CH3OH} equilibrium pressure. Solid symbols: ads. I, open symbols: ads. II. $T_{ads.}$ = 303 K

Fig.5: Differential heats of adsorption of $H_2O_{vap.}$ on beta-1 (♦), beta-2 (●), beta-3 (▼) and beta-silicalite (▲), in comparison with the commercial catalyst beta-10 (■), characterized by Si/Al = 10. Inset: volumetric isotherms, n_{ads} (H_2O molecules/uc) *vs*. p_{H2O} equilibrium pressure. In both q^{diff} *vs.* n_{ads} and n_{ads} *vs.* p_{eq} plots only the first run data (ads. I) are reported. $T_{ads.}$ = 303 K

Fig.6: Integral molar heats of adsorption $[q^{mol}]_p = (Q^{int}/n_{ads})$ as a function of the average crystals size of the catalyst, at two different surface coverage: n_{ads} =2 H_2O molecules/uc (left) and n_{ads} = 4 H_2O molecules/uc (right). $T_{ads.}$ = 303 K

Fig.7: B3LYP/6-31+G(d,p) optimized structures of the clusters adopted to mimic the Lewis site interacting with CH_3OH (*a*) and H_2O molecule (*b*). Binding energies (BE, kJ/mol) corrected for the basis set superposition error. Bonds between Al and the oxygen atom of the adsorbed molecule shown as dotted lines.

Fig.8. FT-IR spectra of beta-1 catalyst after saturation with pyridine followed by evacuation at progressively increasing temperature.

Fig.9. FT-IR spectra of beta-2 catalyst after saturation with pyridine followed by evacuation at progressively increasing temperature.

Fig.10. Effect of time-on-stream on conversion of phenol in alkylation over beta-2 catalyst at four different temperatures.

Fig.11. Effect of time-on-stream on products distribution in alkylation of phenol over beta-2 catalyst. T = 450°C.

Fig.12. Effect of time-on-stream on conversion of phenol in alkylation over beta-3 catalyst at four different temperatures.

Fig.13. Effect of time-on-stream on products distribution in alkylation over beta-3 catalyst. T = 450°C.

Fig.14. Effect of phenol conversion on the anisole/cresols molar ratio in alkylation, at 320°C (black symbols), 390°C (grey symbols) and 450°C (white symbols), for the beta-2 (squares) and beta-3 (triangles) catalysts.

Fig. 15. Effect of time-on-stream on methanol conversion and on products distribution in poly-alkylbenzenes formation over beta-2 catalyst. T = 450°C. Symbols: (◆) methanol conversion; (●) selectivity to toluene, (■) to pentamethylbenzene, (▲) to hexamethylbenzene.

Fig. 16. Effect of time-on-stream on methanol conversion and on products distribution in poly-alkylbenzenes formation over beta-3 catalyst. T = 450°C. Symbols as for Fig.13.

Table 1. Main characteristics and energetics of interaction with H_2O and CH_3OH of the investigated catalysts

Cat.	SiO_2/Al_2O_3 mol ratio	Si/Al mol ratio	Al/uc	av. cryst. size (nm)	SSA (m^2/g)	V_{pTOT} (cm^3/g)	V_{pMicr} (cm^3/g)	Na^+ wt %	q_0 H_2O kJ/mol	q_0 CH_3OH kJ/mol
beta-1	65	130	≈ 0.5	200	481	0.343	0.239	2.42	100	-
beta-2	77	154	≈ 0.4	100	559	0.627	0.266	0.07	160	50
beta-3	65	130	≈ 0.5	590	565	0.324	0.299	0.01	160	50
beta-silical.	255	510	<0.1	450	529	0.311	0.270	<0.001	80	-
beta-10	4.9	9.8	≈ 6	50	360	-	-	-	165	-

Table 2: Summary of the most important IR spectroscopic features.

IR feature	beta-1 frequency (cm^{-1})	beta-2 frequency (cm^{-1})	beta-3 frequency (cm^{-1})
ν(OH) isolated silanols	3740	3740	3740
ν(OH) internal and /or H-bonded silanols	3670	3580	3500
ν(OH) SiOHAl	Not visible	3615	3613
ν(OH)….OH-CH3	Not reported	3400	2100
A_{comp} maximum	Not reported	Not revealed	2900
First Evans window	Not reported	Not revealed	2720
B_{comp} maximum	Not reported	Not revealed	2500
Second Evans window	Not reported	Not revealed	2000
C_{comp} maximum	Not reported	Not revealed	1600

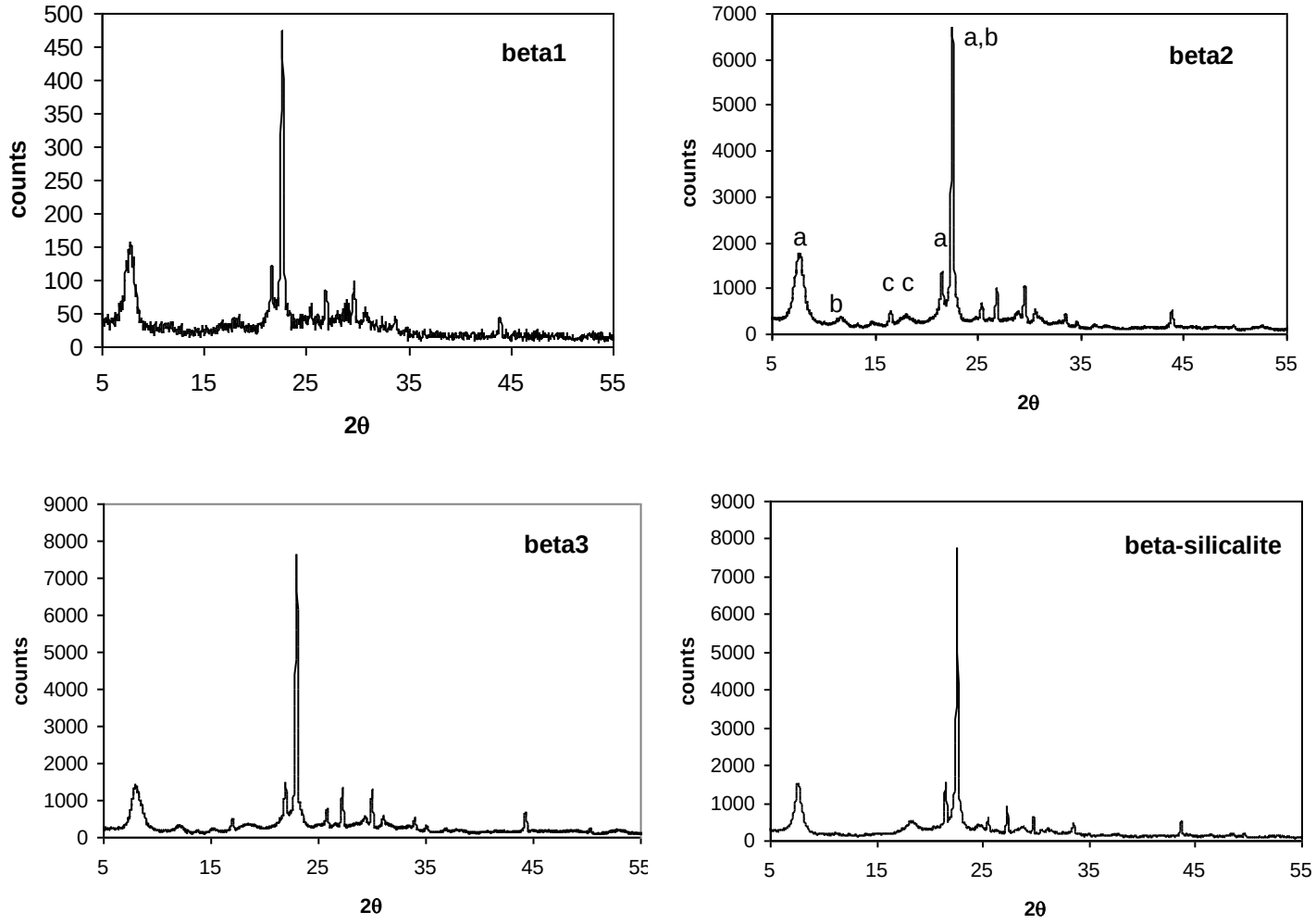

Fig.1

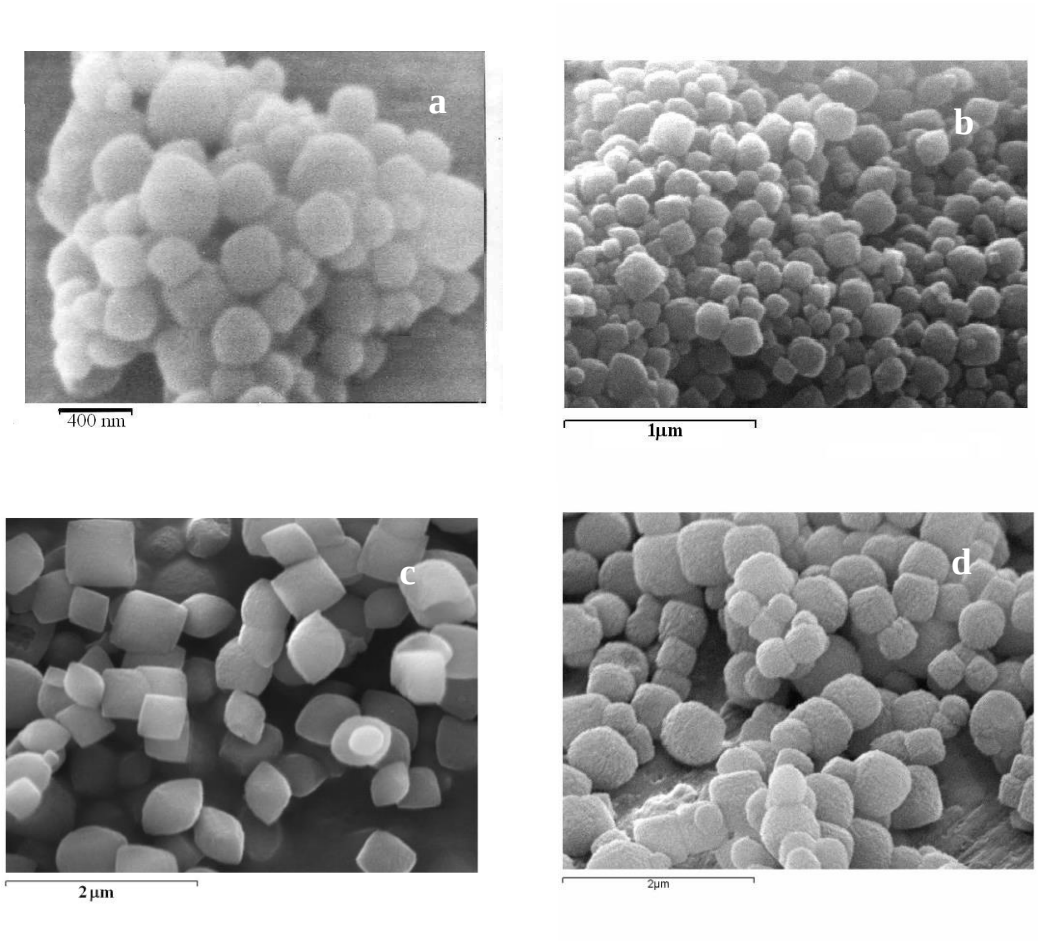

Fig.2

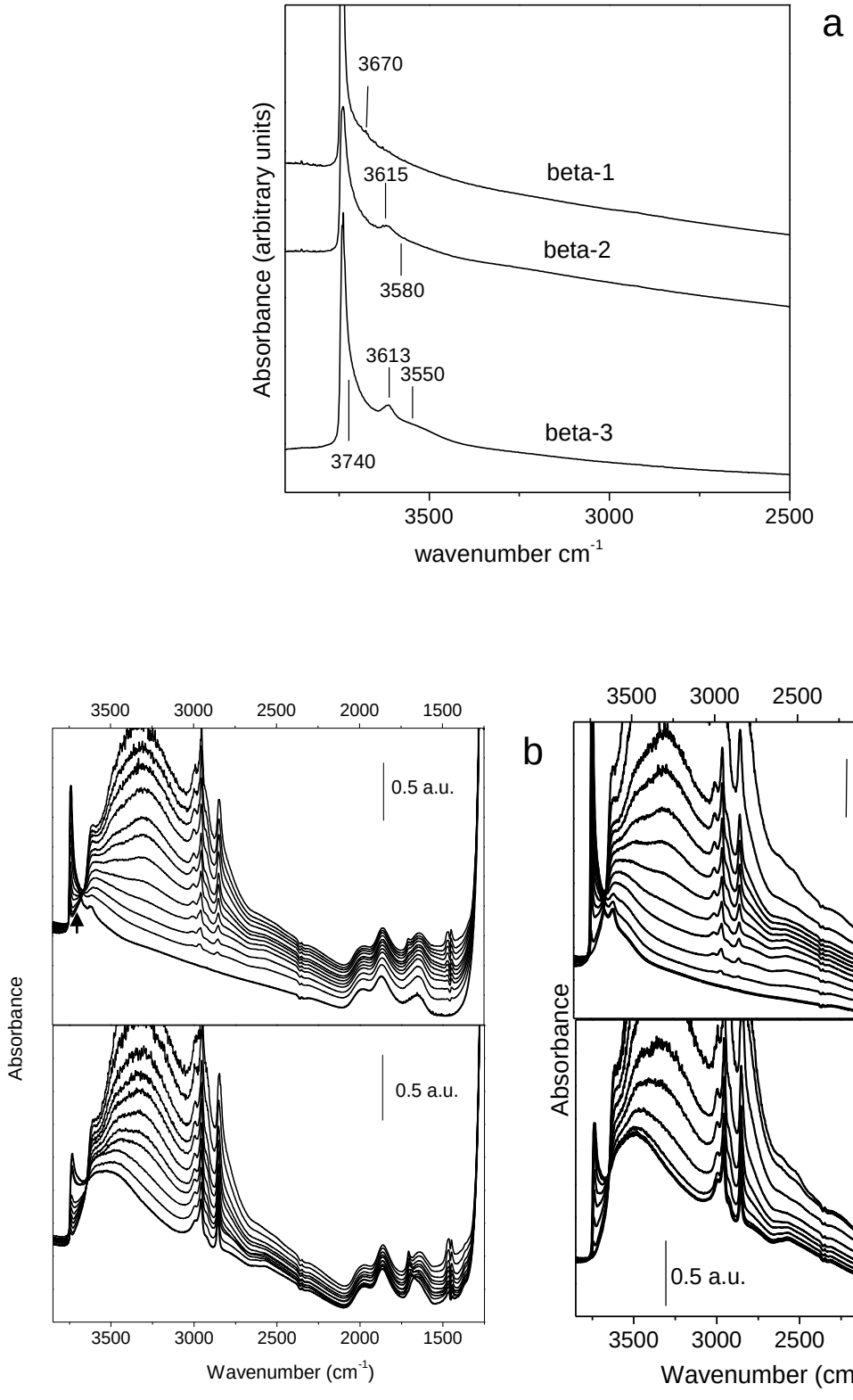
a
3670
3615
3580
3613
3550
3740
beta-1
beta-2
beta-3
Absorbance (arbitrary units)
3500
3000
2500
wavenumber cm-1
b
0.5 a.u.
0.5 a.u.
0.5 a.u.
0.5 a.u.
Absorbance
Wavenumber (cm-1)
Wavenumber (cm-1)

Fig.3

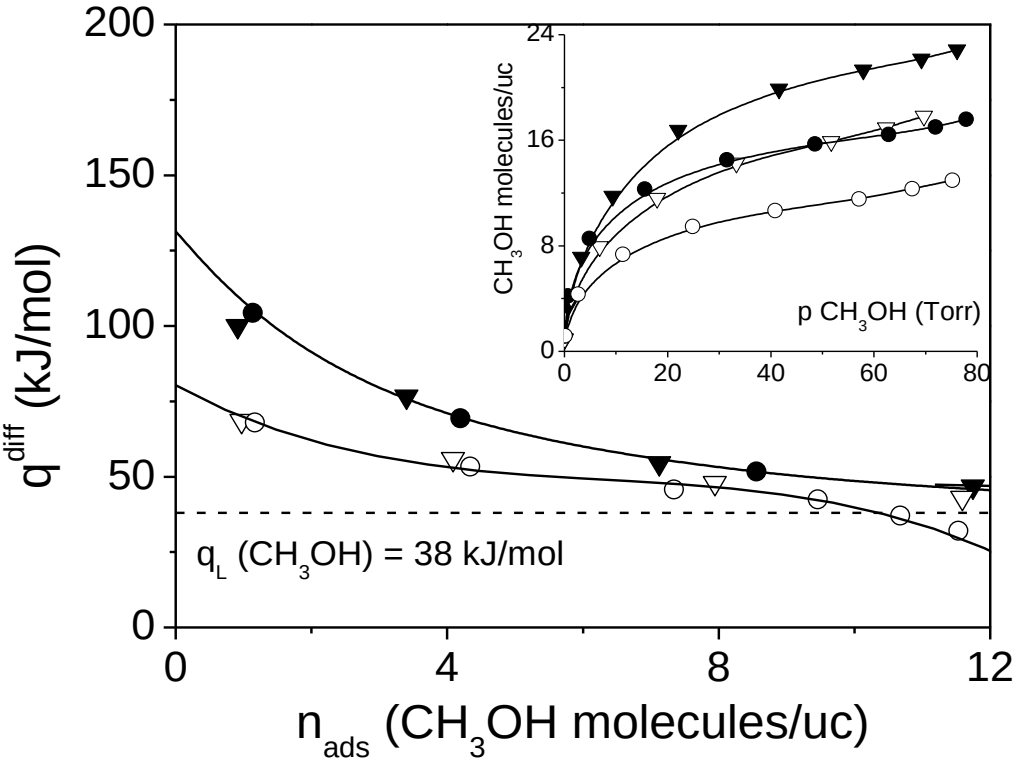
200
150
100
50
0
q^{diff} (kJ/mol)
0
4
8
12
n_{ads} (CH_3OH molecules/uc)
q_L (CH_3OH) = 38 kJ/mol
24
16
8
0
CH_3OH molecules/uc
0
20
40
60
80
p CH_3OH (Torr)

Fig4

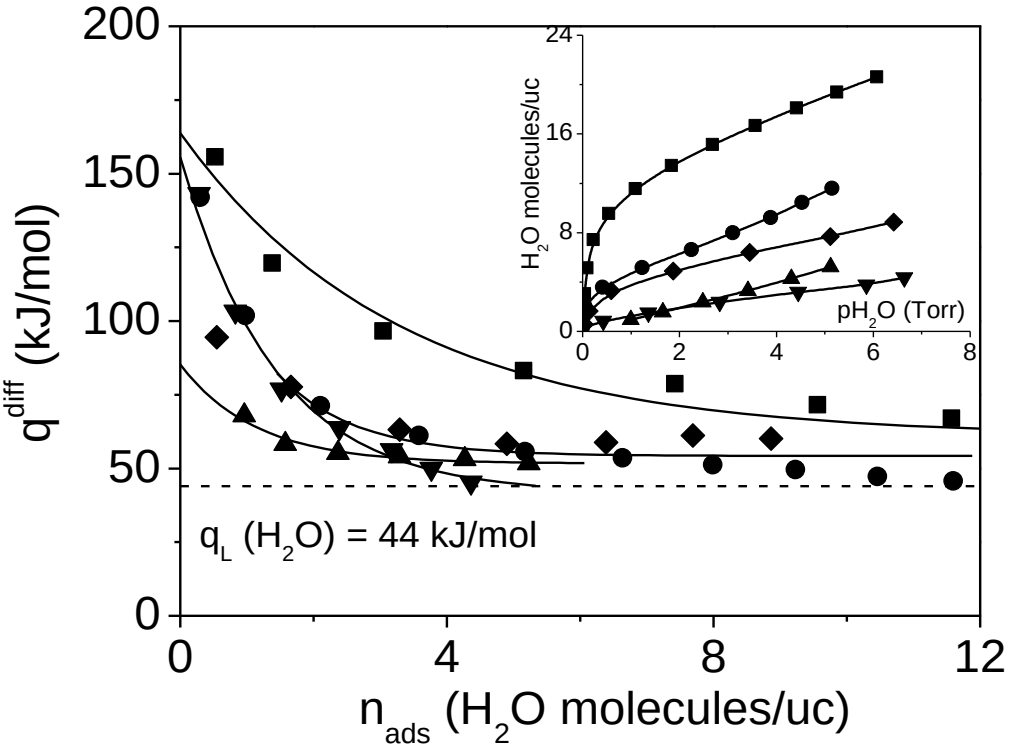
200
150
100
50
0
q^{diff} (kJ/mol)
0
4
8
12
n_{ads} (H_2O molecules/uc)
q_L (H_2O) = 44 kJ/mol
24
16
8
0
H_2O molecules/uc
0
2
4
6
8
pH_2O (Torr)

Fig.5

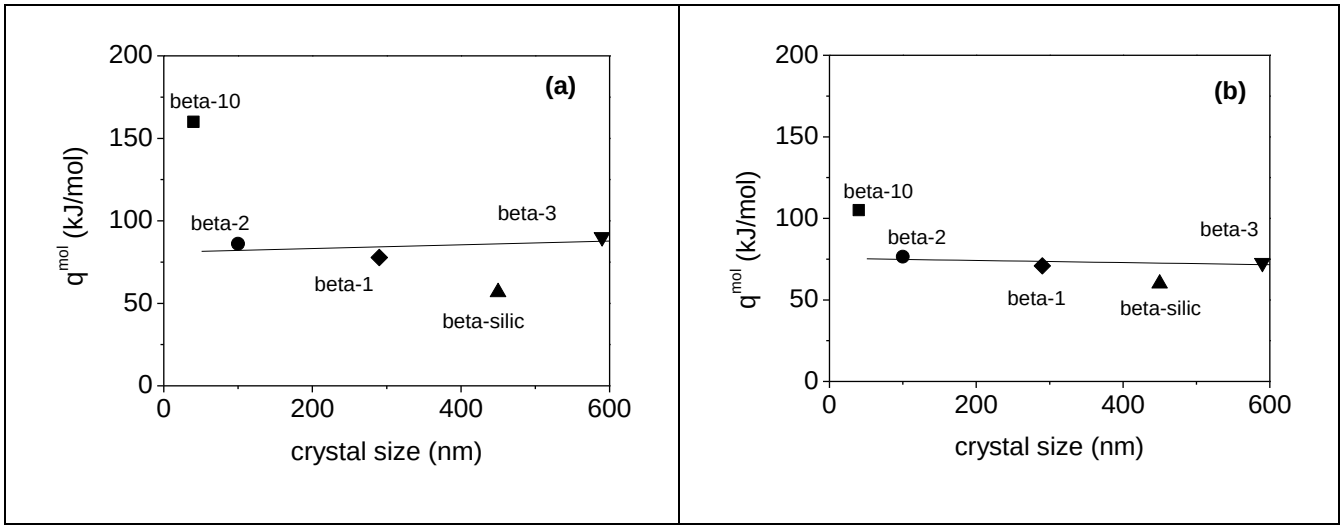
(a)
beta-10
beta-2
beta-1
beta-3
beta-silic
q^{mol} (kJ/mol)
crystal size (nm)
0
50
100
150
200
0
200
400
600
(b)
beta-10
beta-2
beta-1
beta-3
beta-silic
q^{mol} (kJ/mol)
crystal size (nm)

Fig.6

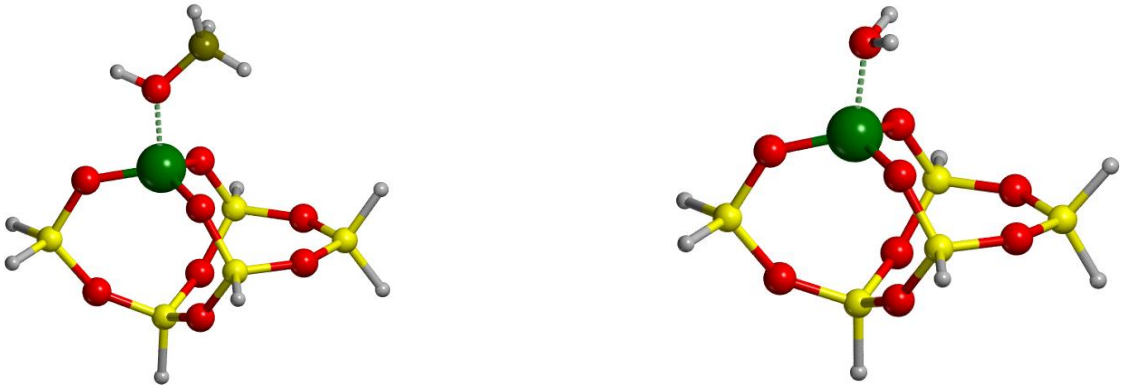

(a) BE = 125 kJ/mol	(b) BE = 110 kJ/mol

Fig.7

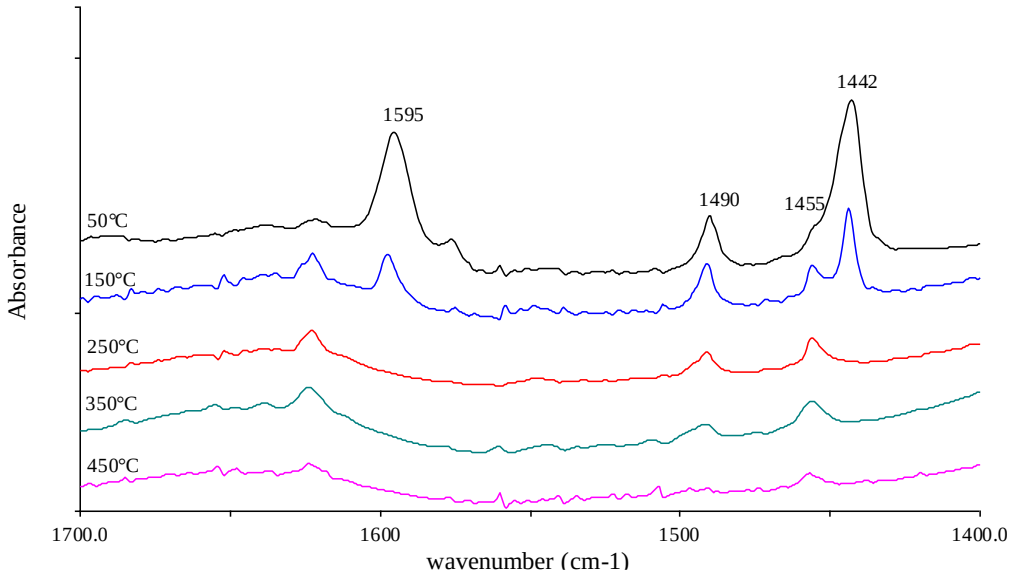

Fig.8

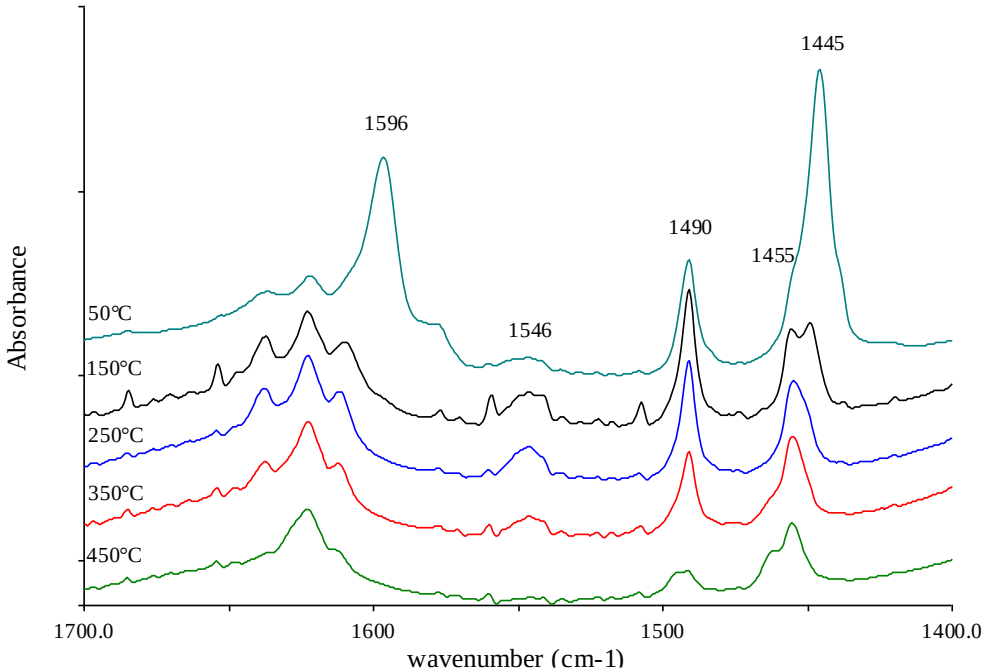
Absorbance
1596
1546
1490
1455
1445
50℃
150℃
250℃
350℃
450℃
1700.0
1600
1500
1400.0
wavenumber (cm-1)

Fig.9

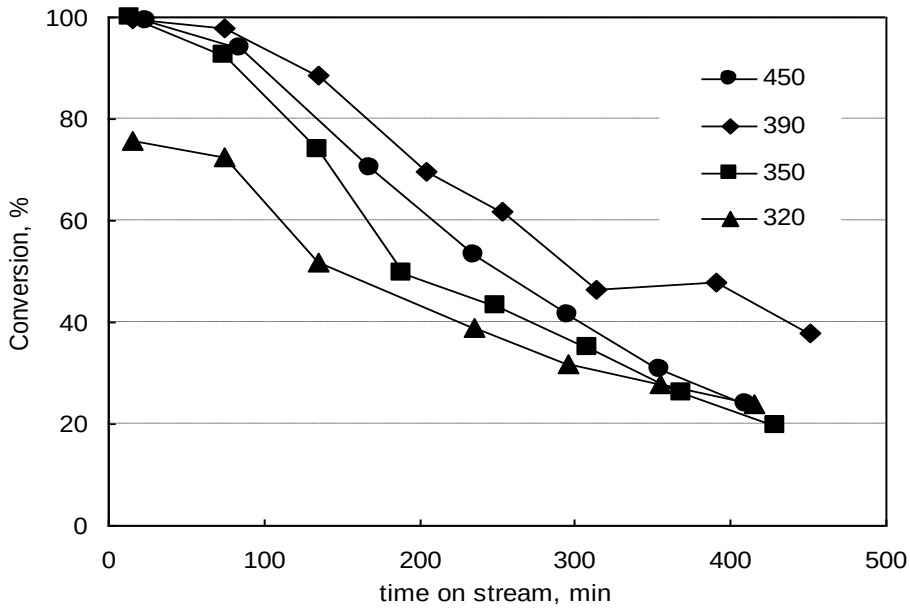
Conversion, %
100
80
60
40
20
0
0
100
200
300
400
500
time on stream, min
450
390
350
320

Fig.10

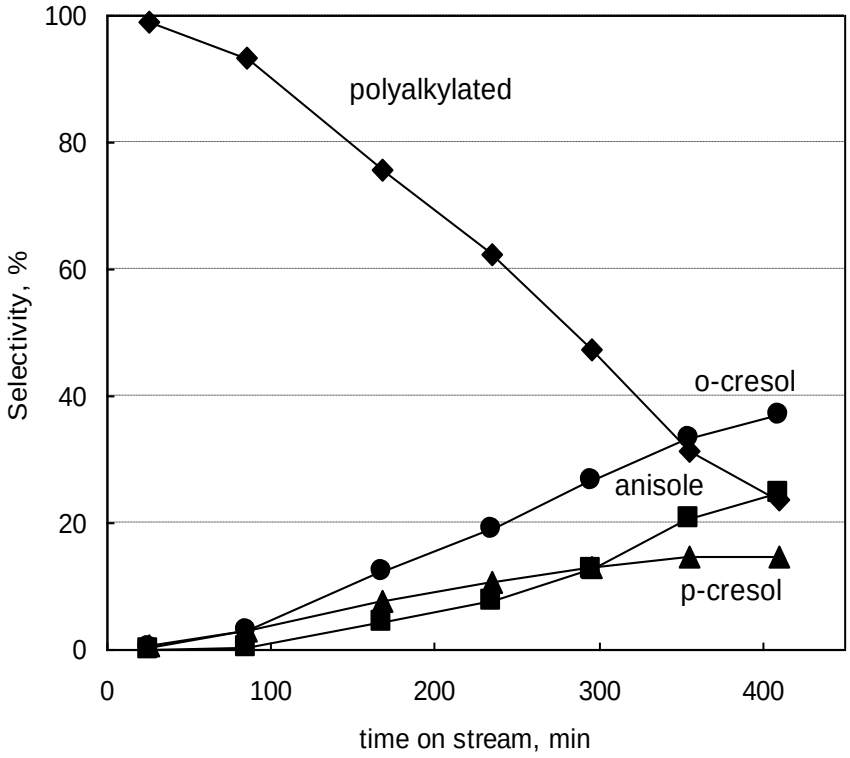
100
80
60
40
20
0
Selectivity, %
polyalkylated
o-cresol
anisole
p-cresol
0
100
200
300
400
time on stream, min

Fig.11

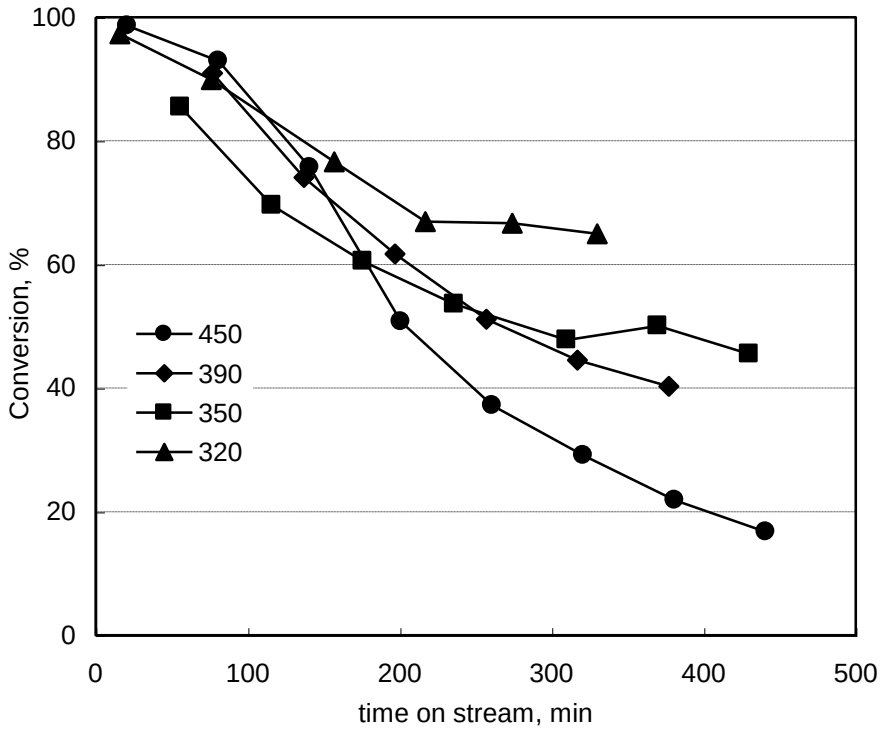
100
80
60
40
20
0
Conversion, %
450
390
350
320
0
100
200
300
400
500
time on stream, min

Fig.12

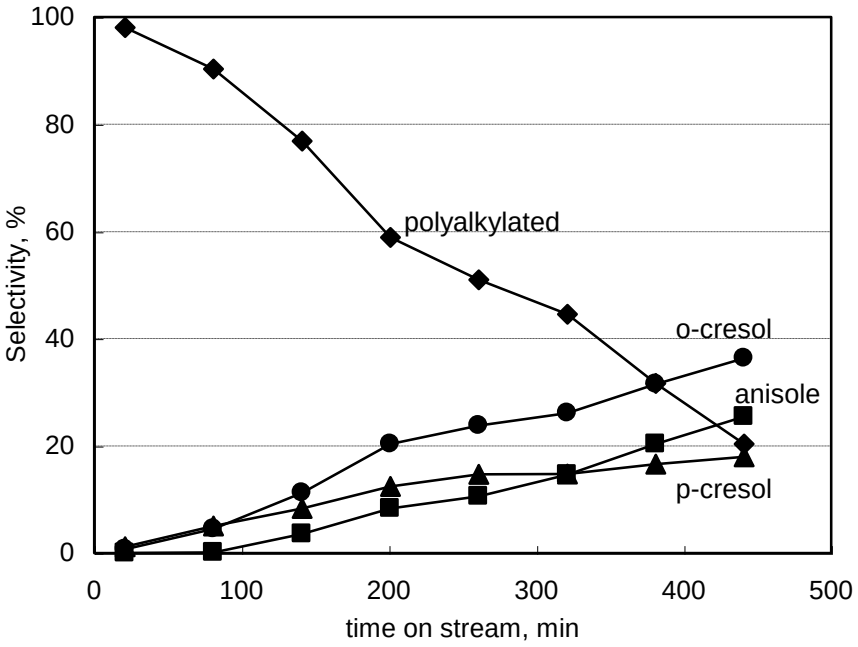
Selectivity, %
time on stream, min
polyalkylated
o-cresol
anisole
p-cresol
0
20
40
60
80
100
0
100
200
300
400
500

Fig.13

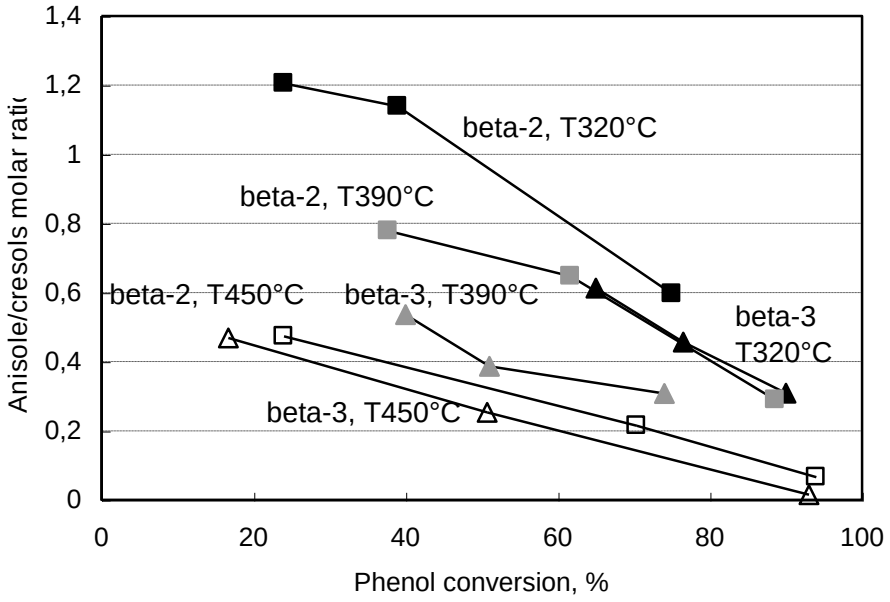
Anisole/cresols molar ratio
Phenol conversion, %
beta-2, T320°C
beta-2, T390°C
beta-2, T450°C
beta-3, T390°C
beta-3
T320°C
beta-3, T450°C
0
0,2
0,4
0,6
0,8
1
1,2
1,4
0
20
40
60
80
100

Fig.14

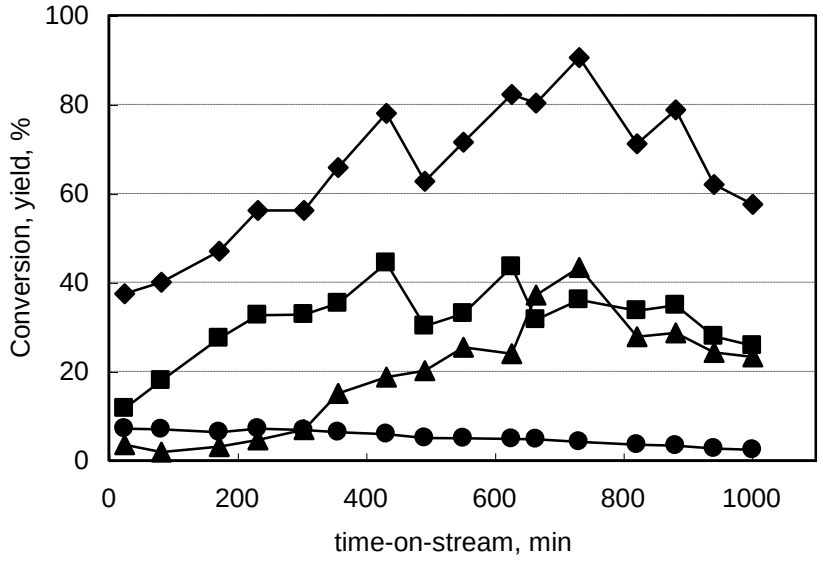
100
80
60
40
20
0
Conversion, yield, %
0
200
400
600
800
1000
time-on-stream, min

Fig.15

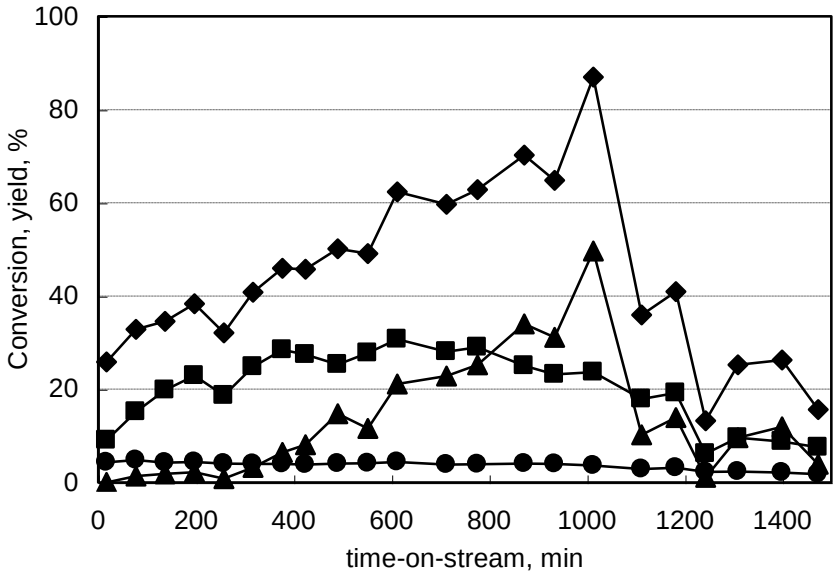
100
80
60
40
20
0
Conversion, yield, %
0
200
400
600
800
1000
1200
1400
time-on-stream, min

Fig.16